J. Fluid Mech. (1994), *vol.* 277, *pp.* 271–301

Direct simulation of initial value problems for the motion of solid bodies in a Newtonian fluid. Part 2. Couette and Poiseuille flows

By J. FENG[1], H. H. HU[2] AND D. D. JOSEPH[1]

[1] Department of Aerospace Engineering and Mechanics *and* The Minnesota Supercomputer Institute, University of Minnesota, Minneapolis, MN 55455–0153, USA

[2] Department of Mechanical Engineering and Applied Mechanics, University of Pennsylvania, Philadelphia, PA 19104–6315, USA

(Received 20 September 1993 and in revised form 11 May 1994)

This paper reports the results of a two-dimensional finite element simulation of the motion of a circular particle in a Couette and a Poiseuille flow. The size of the particle and the Reynolds number are large enough to include fully nonlinear inertial effects and wall effects. Both neutrally buoyant and non-neutrally buoyant particles are studied, and the results are compared with pertinent experimental data and perturbation theories. A neutrally buoyant particle is shown to migrate to the centreline in a Couette flow, and exhibits the Segré–Silberberg effect in a Poiseuille flow. Non-neutrally buoyant particles have more complicated patterns of migration, depending upon the density difference between the fluid and the particle. The driving forces of the migration have been identified as a wall repulsion due to lubrication, an inertial lift related to shear slip, a lift due to particle rotation and, in the case of Poiseuille flow, a lift caused by the velocity profile curvature. These forces are analysed by examining the distributions of pressure and shear stress on the particle. The stagnation pressure on the particle surface are particularly important in determining the direction of migration.

1. Introduction

The problem of particle motion in shear flows has received considerable attention in the past thirty years. The pioneering experiments of Segré & Silberberg (1961, 1962) have spawned numerous research efforts, leading to the conclusion that in shear flows of a Newtonian fluid solid particles migrate across streamlines in the presence of walls, velocity profile curvature and buoyancy forces, unless the particle is so small that its relative motion with respect to the fluid is negligible (Goldsmith & Mason 1966). The 'anomalous' motion observed is attributed to the nonlinear effect of inertia. Comprehensive reviews of experimental and theoretical works have been given by Brenner (1966), Cox & Mason (1971), Leal (1980) and Feuillebois (1989).

Theoretical works for understanding lateral migrations use perturbation theory and direct numerical simulations. In the present paper, we report the results of a two-dimensional direct simulation of the motion of a single circular particle in a Couette and a Poiseuille flow. The numerical code is based on a finite element method using the POLYFLOW Navier–Stokes solver and has been used to simulate complex particle motions of sedimenting spheres and ellipses (Hu, Crochet & Joseph 1992; Feng, Hu & Joseph 1994; Huang, Feng & Joseph 1994; Liu *et al.* 1993). Because the fluid flow is

computed from the fully nonlinear Navier–Stokes equations, and the motion of the particles is determined by Newton's equations for rigid bodies under the action of the hydrodynamic forces and torques arising from the fluid flow, we are able to simulate particle motion exactly up to the accuracy that our numerical method allows.

Our numerical package is described by Hu *et al.* (1992) and will not be discussed here, except to say that we use a semi-implicit method on a triangular unstructured grid which is laid down anew at each time step. It will be better if simulations of this kind can be carried out in three dimensions. The two-dimensional simulation does not allow for unambiguous comparison with experiments and with perturbation theories that have been carried out in three dimensions. Feng *et al.* (1994) showed that many features of the results of two-dimensional simulations apply qualitatively to three-dimensional experiments, but the comparisons are imperfect and can lead to serious errors.

In this paper, we have gone further than before in interrogating our code for the underlying fluid mechanics controlling the side forces, the turning couples and the effects of the wall on the migration and equilibrium positions of the circular particle. The role of 'stagnation' points and separation points in controlling the viscous and pressure forces on a body moving in a viscous fluid can be clarified by asking the right questions of a good simulation, and we can hope that the answer we get are not so dramatically different in two and three dimensions.

In the past, all theoretical studies of particle migrations have been based on perturbation theories, and the ones of interest here are for spherical particles in planar shear flows (three-dimensional problems). The value of these perturbation studies in understanding migration across streamlines can scarcely be overestimated. The results of these studies find application in different contexts and, in particular, are used to model lift forces in two-phase flows. However, the perturbation theories have very restricted domains of applicability and because of the heavy analysis required have not informed us particularly well about the fundamental fluid dynamic mechanisms underway. It is therefore of value to see how well perturbation theories can represent the motion of particles in the usual conditions in which the restrictive assumptions of the perturbation theories do not hold. This kind of comparison is one of the tasks taken up here.

Among many perturbation theories the ones by Bretherton (1962*a*), Saffman (1965), Cox & Brenner (1968), Ho & Leal (1974), Cox & Hsu (1977) and Vasseur & Cox (1976) need to be mentioned. The first two papers are different from the others, because they are zeroth-order theories and are posed in an unbounded domain in which the inertia of the far field cannot be ignored. This is a well-known case in which Stokes flow near the body is matched with Oseen flow far away. The lift forces in such theories depend on the viscosity and are linear in the velocity. Bretherton (1962*a*) is the only one to work strictly in two dimensions, and he finds that the lift Λ per unit length on the cylinder is given by

$$\Lambda = 84.63\rho\nu U\left(\frac{1}{\ln Re}\right)^2, \tag{1.1}$$

where ν is the kinematic viscosity; U is the slip velocity of the particle (the particle velocity minus the undisturbed velocity at the particle centre); and $Re = Ga^2/\nu$, G being the shear rate and a the circle radius.

Saffman's (1965) lift on a spherical particle of radius a in a shear flow with rate G is

$$\Lambda = 6.46\rho U a^2 (G\nu)^{1/2} = 6.46\rho\nu U a\, Re^{1/2}. \tag{1.2}$$

Obviously, there is a huge difference between the lift (1.1) in two dimensions and the lift (1.2) in three dimensions. This difference can be traced to the fact that the effects of inertia in the far field are such as to make steady Stokes flow impossible in an unbounded region in two dimensions. Recently, Saffman's theory has been extended to allow relatively strong shear (McLaughlin 1991), quadratic velocity profiles (Schonberg & Hinch 1989) and bounding walls outside the Oseen region (McLaughlin 1993; Schonberg & Hinch 1989).

The other theories are different in principle because they are in effectively bounded domains with the parameters arranged in such a way that a uniformly valid Stokes flow can be obtained at zeroth order. Of course, no lateral migration will occur in the Stokes flow, and the lift force is obtained at the next order where it is determined by inertia alone without any explicit dependence on viscosity. For example, Ho & Leal (1974) found that a neutrally buoyant particle in a shear flow experiences a lift

$$\Lambda = \rho U_w^2 a^2 \kappa^2 G_1(s), \tag{1.3}$$

where $s = \delta/L$ is the fractional distance from the wall, L being the channel width; $\kappa = a/L$ is the dimensionless radius of the sphere; $G_1(\cdot)$ a function found by Ho & Leal; and U_w is the wall velocity defined in figure 1. The formula (1.3) is quadratic in velocity and independent of viscosity. This lift arises from inertia alone at first order in a perturbation of a flow which is dominated by viscosity everywhere at zeroth order.

The low-Reynolds-number formulae (1.1) and (1.2) for the lift on a particle in an unbounded fluid are seen to be vastly different from formulae like (1.3) given by Cox & Brenner (1968), Ho & Leal (1974), Cox & Hsu (1977) and Vasseur & Cox (1976) which hold in 'effectively' bounded domains, when the particle is so close to the wall that it is dominated by viscosity at the lowest order. The condition for this was given by Cox & Brenner (1968) as

$$Re/\kappa \ll 1 \tag{1.4}$$

A strictly bounded domain, say a spherical shell, can be 'effectively' unbounded when (1.4) does not hold, because the inertia of the far field enters into the dynamics of the particle at the lowest order, as it does in the analysis of Bretherton (1962*a*) and Saffman (1965).

To understand the difference in the lift formulae, it is necessary to look at mathematical details for flows in effectively bounded domains. When (1.4) holds, one need consider only the inner expansion in the viscous region to calculate the first term in the expansion for the migration velocity in powers of $Re = aV/\nu$, where V is a characteristic velocity defined differently in different problems. Following the approach of Cox & Brenner (1968), one expands $\boldsymbol{v}$, p, $\boldsymbol{U}$ and $\boldsymbol{\Omega}$ as power series in Re: $\boldsymbol{v}$ and p are the disturbance velocity and pressure fields in a system of coordinates moving but not rotating with the particle; $\boldsymbol{U}$ and $\boldsymbol{\Omega}$ are the velocity and angular velocity of the particle in a fixed reference frame. The disturbance flow satisfies

$$\left.\begin{aligned} \nabla^2 \boldsymbol{v} - \nabla p &= Re[\boldsymbol{v}\cdot\nabla\boldsymbol{v} + \boldsymbol{v}\cdot\nabla\boldsymbol{V} + \boldsymbol{V}\cdot\nabla\boldsymbol{v}] \quad (r > 1), \\ \boldsymbol{v} &= \boldsymbol{\Omega}\wedge\boldsymbol{r} - \boldsymbol{V} \quad (r = 1), \end{aligned}\right\} \tag{1.5}$$

where lengths have been made dimensionless by the particle radius a; $\boldsymbol{V} = \tilde{\boldsymbol{U}} - \boldsymbol{U}$ is the velocity of the fluid at infinity seen by an observer fixed on the particle, $\tilde{\boldsymbol{U}}$ being the velocity of the fluid in a fixed frame. $\boldsymbol{\Omega}$ and $\boldsymbol{U}$ will be determined by hydrodynamic torques and forces alone, which sum to zero since prescribed forces are zero and accelerations are presumed negligible. If x is the direction of the bulk motion, $\boldsymbol{U}\cdot\boldsymbol{e}_y$ is the lateral drift velocity whose behaviour is at issue.

Proceeding by identification as in regular perturbations, one finds that

$$\left.\begin{aligned} \nabla^2 \boldsymbol{v}_0 &= \nabla p_0 \quad (r > 1), \\ \boldsymbol{v}_0 &= \boldsymbol{\Omega}_0 \wedge \boldsymbol{r} - \boldsymbol{V}_0 \quad (r = 1), \end{aligned}\right\} \tag{1.6}$$

where $\boldsymbol{V}_0 = \tilde{\boldsymbol{U}} - \boldsymbol{U}_0$ and

$$\left.\begin{aligned} \nabla^2 \boldsymbol{v}_1 - \nabla p_1 &= \boldsymbol{v}_0 \cdot \nabla \boldsymbol{v}_0 + \boldsymbol{V}_0 \cdot \nabla \boldsymbol{v}_0 + \boldsymbol{v}_0 \cdot \nabla \boldsymbol{V}_0 \quad (r > 1), \\ \boldsymbol{v}_1 &= \boldsymbol{\Omega}_1 \wedge \boldsymbol{r} + \boldsymbol{U}_1 \quad (r = 1). \end{aligned}\right\} \tag{1.7}$$

The velocity fields $\boldsymbol{v}_0$ and $\boldsymbol{v}_1$ are divergence free and vanish on bounding walls and at infinity. Since there is no lateral drift in Stokes flow (Bretherton 1962*b*), $\boldsymbol{U}_0 \cdot \boldsymbol{e}_y = 0$ and $\boldsymbol{U} \cdot \boldsymbol{e}_y = Re\, \boldsymbol{U}_1 \cdot \boldsymbol{e}_y$. Cox (1965) found a method of computing $\boldsymbol{U}_1 \cdot \boldsymbol{e}_y$ without first calculating $\boldsymbol{v}_1$ and p_1. An auxiliary Stokes flow problem for $\boldsymbol{u}$ is defined such that $\boldsymbol{u} = \boldsymbol{e}_y$ at $r = 1$ and $\boldsymbol{u} = \boldsymbol{0}$ on bounding walls and at $r = \infty$. This leads to a formula for the drifting velocity (equation (2.20) of Ho & Leal 1974):

$$\boldsymbol{U}_1 \cdot \boldsymbol{e}_y = -\frac{1}{6\pi} \int [\boldsymbol{v}_0 \cdot \nabla \boldsymbol{v}_0 + \boldsymbol{V}_0 \cdot \nabla \boldsymbol{v}_0 + \boldsymbol{v}_0 \cdot \nabla \boldsymbol{V}_0] \cdot \boldsymbol{u}\, \mathrm{d}V. \tag{1.8}$$

This formula arises from certain symmetries and from the fact that there are no prescribed lateral forces on the particle. This equation shows that the lateral drift in a viscously dominated flow satisfying (1.4) is determined by the inertia of the Stokes flows.

We draw the reader's attention to the fact that though there is a great difference between two and three dimensions in an unbounded domain (cf. (1.1) and (1.2)), no such great difference exists in effectively bounded domains. The equations following (1.4) make no distinction between two- and three-dimensional domains. Perturbation analyses like those given by Ho & Leal (1974) and by Vasseur & Cox (1976) could and should be carried out for two-dimensional problems.

Various cases considered by Ho and Leal (1974) and Vasseur & Cox (1976) can be framed in terms of (1.8). In the neutrally buoyant case of Couette flow studied by Ho & Leal, both $\boldsymbol{V}_0$ and $\boldsymbol{v}_0$ are proportional to the wall velocity U_w, leading to the quadratic lift (1.3). Non-neutrally buoyant flows are considered by Vasseur & Cox to examine the effects of 'slip' on the lateral migration of spheres. The velocity V used in Re is the magnitude of the fall velocity of the sphere, which is positive when the sphere is heavier than the fluid.

The relation between the lateral drift and the lift forces in the cases in which (1.4) is satisfied can be partly understood from dimensional considerations using the perturbation equations (1.7) in dimensional form, with μ multiplying $\boldsymbol{v}_1$ (now dimensional) and ρ multiplying the right-hand side. The dimensional lift is then independent of the viscosity because the stress $\mu(\nabla \boldsymbol{v}_1 + \nabla \boldsymbol{v}_1^T)$ which gives rise to the lift is determined by the inertia of the flow field prescribed at zeroth order and a^2 times the stress is proportional to lift, as in (1.3). This implies that $\boldsymbol{v}_1$ and therefore $\boldsymbol{U}_1 \cdot \boldsymbol{e}_y$ is proportional to $1/\mu a$ times the lift, so that $1/\mu$ enters into the formula for the lateral drift when the lift is independent of μ.

Another restriction of the perturbation theories in bounded domains is associated with the methods used for solution which require that the particle should not be too close to the wall. Ho & Leal (1974) used the method of reflections of Lorentz, whereas Vasseur & Cox (1976) used a point-force approximation to solve the perturbation equations. Ho & Leal (1974) require $Re/\kappa^2 \ll 1$, a more restrictive condition than

$Re/\kappa \ll 1$ required by Vasseur & Cox (1976). Both methods fail very near to a wall, and they give dramatically different results there (see figure 5 in Vasseur & Cox 1976).

We may summarize the restrictions of the perturbation equations used by Cox & Brenner (1968), Ho & Leal (1974), Cox & Hsu (1977) and Vasseur & Cox (1976) as $Re \ll 1$, $\kappa = a/L \ll 1$, $a/\delta \ll 1$ and $a/(L-\delta) \ll 1$, where δ is the distance from the wall; that is, small Reynolds numbers, small particles and not too small distances from the wall are required. The condition $Re/\kappa \ll 1$ leads to a lift independent of viscosity, an asymptotic result incompatible with (1.1), (1.2) and conditions usually found in practice. In fact, Vasseur & Cox (1977) relaxed this condition for sedimentation without shear and found lift forces that do depend on the viscosity. The restriction of perturbation theories are such as to leave open only the smallest of windows in which to examine the mechanics of motion. Fortunately the results of perturbation theories appear to hold when the assumptions for their validity do not.

The restrictions which apply to perturbation theories do not apply to direct numerical simulations. We are able to compute the motions of large and small particles at Reynolds numbers in the hundreds. The transient motions and bifurcation scenarios which are neglected in perturbation theories are accommodated in the simulations. The effects of viscosity and inertia on lift forces and lateral drift are not compromised by the assumptions which are required in different perturbation theories. In fact, viscous contributions to the lateral force in bounded domains can be appreciable, about half the contribution from inertia for a sedimenting particle (see Liu *et al.* 1993). The lack of validity of perturbation theories near a wall does not apply to direct simulation. The effects of the wall on hydrodynamically induced rotations, the lift force, the lateral particle velocity and equilibrium positions for the particles (Segré–Silberberg effect) can be obtained from direct simulation without compromising assumptions. A thoughtful interrogation of a good simulation, like that given in §§2 and 3, can lead to understandings of the basic fluid mechanics that could never be revealed in the small window of parameters in which perturbation theories apply.

The restriction of simulations to two-dimensional problems has already been relaxed in some recent simulations of particle-in-fluid motions (Unverdi & Tryggvason 1992). Undoubtedly, the formulae for lift, drag, lateral drift velocity and torque derived from perturbations are both useful and gratifying. Such formulae have not yet been produced by direct simulations. We believe that this situation is also temporary. There is no reason why 'empirical' formulae of the type used in engineering which correlate experimental data cannot be generated from the data produced by numerical simulations. We hope to generate such formulae for the lift, lateral velocity and other functionals of the solution given by direct simulation in the future.

In the following sections, we will present the results of simulations on neutrally and non-neutrally buoyant particles migrating in Couette and Poiseuille flows. Our results will be compared with relevant experiments and the two kinds of perturbation theories just described. We will refer to theories like those of Bretherton (1962*a*) and Saffman (1965) on effectively unbounded domains as *viscous theories*; theories like those of Cox & Brenner (1968), Ho & Leal (1974), Cox & Hsu (1977) and Vasseur & Cox (1976) on effectively bounded domains will be called *inertial theories*.

2. Particle migration in a planar Couette flow

We now consider the lateral migration of a circular particle in a simple shear flow. The particle's radius is a and the width of the channel is $L = 8a$ so that $\kappa = a/L = 0.125$. It will be easier to discuss the results in a coordinate system in which both walls

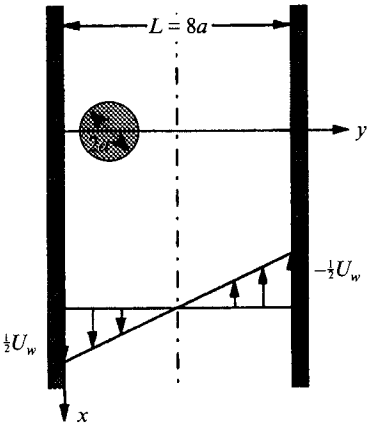

FIGURE 1. Migration of a particle in a simple shear flow between walls. $\kappa = 0.125$, $\mathcal{R}_p = 0.625$.

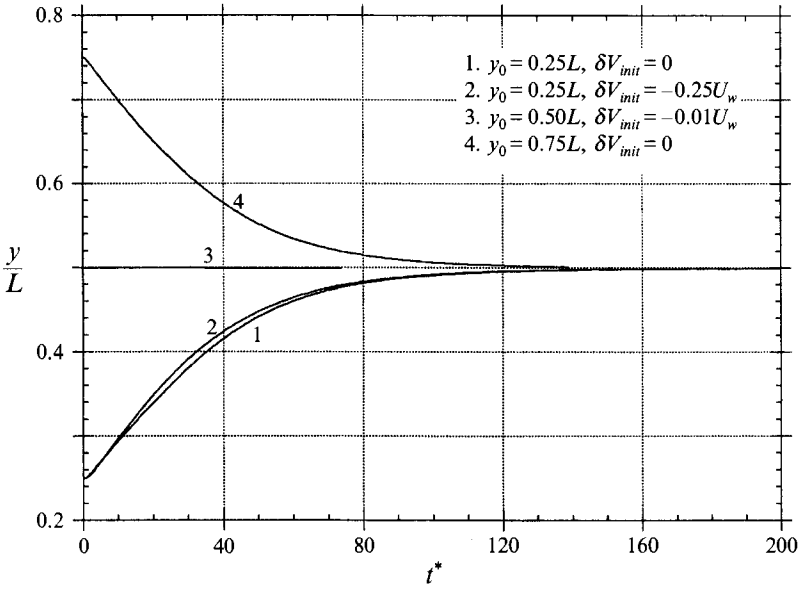

FIGURE 2. Lateral migration of neutrally buoyant particles released at $y_0 = 0.25L$ and $0.75L$ in the Couette flow shown in figure 1. δV_{init} is the initial slip velocity. The dimensionless time is $t^* = U_w t/L$.

are moving in opposite directions at $\frac{1}{2}U_w$ (figure 1). If we use $[L, U_w, L/U_w, \rho_f U_w^2]$ as scales for length, velocity, time and pressure, the following parameters appear in the equations governing fluid and particle motions: bulk Reynolds number $\mathcal{R}_b = U_w L/\nu$, Froude number $Fr = gL/U_w^2$, the solid–fluid density ratio $\rho = \rho_s/\rho_f$ and the geometric ratio κ. Fr and ρ are relevant only when the particle is non-neutrally buoyant. For most of the calculations in this section, we use $\mathcal{R}_b = 40$. A particle Reynolds number can be defined as $\mathcal{R}_p = U_w a^2/(\nu L) = 0.625$. Our simulation does not satisfy the small-$\mathcal{R}_p$ condition required for validity of perturbation theories of the viscous type or inertial type. The condition $\mathcal{R}_p \ll \kappa$ of Cox & Brenner (1968) or $\mathcal{R}_p \ll \kappa^2$ of Ho & Leal (1974) is also not satisfied. The results of our simulation and comparison with other works will be presented separately for neutrally buoyant and non-neutrally buoyant particles.

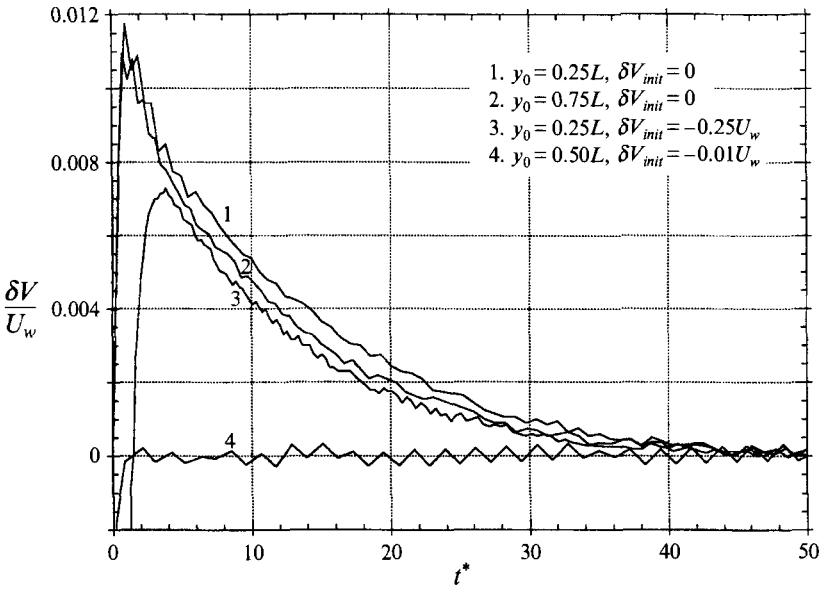

FIGURE 3. Relaxation of the slip velocity δV of particles migrating in a plane Couette flow. $\delta V > 0$ when the particle is leading the fluid in the left half ($y < \frac{1}{2}L$). The sign of δV has been changed for curve 2. The small wiggles are a numerical effect.

2.1. *Neutrally buoyant particles*

Our simulation shows that a neutrally buoyant particle always migrates to the centre of the channel, regardless of initial position and velocity (figure 2). In other words, the centre of the channel is a global attractor of trajectories of a neutrally buoyant particle just as in the case of a heavy particle settling under gravity (Feng *et al.* 1994). The slight asymmetry of the trajectories starting at $y_0 = \frac{1}{4}L/4$ and $\frac{3}{4}L$ (curves 1 and 4 in figure 2) is due to the asymmetry in the mesh. The perturbation solutions of Ho & Leal (1974) and Vasseur & Cox (1976) also predict that the centre is a stable equilibrium, but the mechanisms driving lateral migration are more readily identified in the simulation and are not entirely inertial (see (1.3) and (1.4)).

We have found that after an initial transient the particle is forced to lead the local undisturbed velocity for all cases. The difference between the particle velocity and the undisturbed velocity at the centre of the particle is the slip velocity δV. In figure 3 we have plotted the slip velocity δV normalized by the wall velocity U_w. Since x increases downward, positive slip is indicated by $\delta V > 0$ on the left side of the channel and $\delta V < 0$ on the right side ($y > \frac{1}{2}L$). The sign of δV has been changed for curve 2. In principle, curve 1 should be the same as curve 2; the difference between them is a measure of the inaccuracy of our numerical solution. In the cases computed, the angular velocity rapidly relaxes from zero to the same final value, which is about 47% of the constant shear rate of the undisturbed flow field. In other words, the particle rotates with the local angular velocity of the flow field to within a small correction. This is a well-known result in Stokes flow (Cox, Zia & Mason 1968). Ho & Leal (1974) obtained a similar result for a small sphere in a slow Poiseuille flow.

The migration velocity of the particle depends slightly on initial conditions at the early stage of migration (figure 4). The analytical result of Vasseur & Cox (1976) for an effectively bounded domain is also shown for comparison. Their three-dimensional results are for small spheres in a slow flow, and their analysis does not address

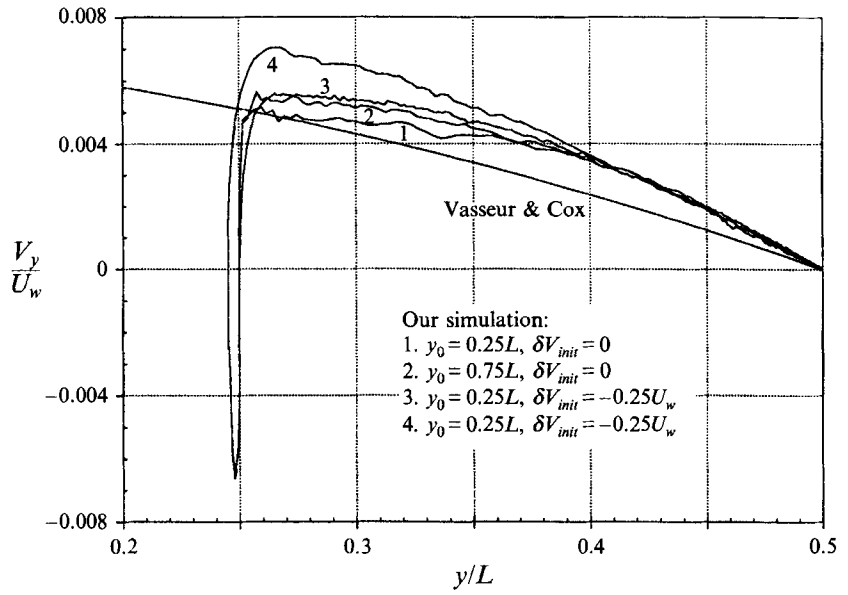

FIGURE 4. Comparison of the migration velocity predicted by our simulation and the theoretical result of Vasseur & Cox (1976) for small spheres. The centreline of the channel is at $y = 0.5L$. The sign of V_y for curve 2 has been changed for comparison. The particle Reynolds number is 1.25 for curve 4 and is 0.625 for the other three curves.

transients. Despite these differences, the trends are alike. Curve 4 is for a larger shear rate with $R_p = 1.25$. It shows that the difference between the simulation and the perturbation theory becomes larger when the inertial effect gets stronger. We also note that immediately after the release, the particle actually acquires a negative transverse velocity and moves a little toward the nearer wall before migrating to the centre. This will be understood as related to the basic mechanisms of the migration discussed later.

As far as we know, the only experiment which can be compared to our simulation is the one by Halow & Wills (1970*b*) in a concentric cylindrical Couette device. They observed that when the inner cylinder rotates, a particle migrates from any initial position to an equilibrium at a small distance inside the centreline of the gap. Their migration curves for particles in three dimensions agree qualitatively with our simulations in two dimensions (figure 5). Because of the difference in geometry, we are unable to construct a characteristic time to compare the speed of migration in both studies. The reader should not interpret figure 5 to mean that the migration speeds agree.

Halow & Wills (1970*a*) then established a semi-empirical model in which the particle lags the fluid in the outer half of the gap and leads the fluid in the inner half. This antisymmetric slip velocity implies that the Saffman lift (see (1.2)) makes the centre line a stable equilibrium position. They calculated the slip velocity by the Lorentz reflection method, which is applicable only to Stokes flows (Happel & Brenner 1965). The particle size and Reynolds number in their experiment ($\kappa = 0.179$, bulk Reynolds number $R_b = U_w L/\nu = 50$) are rather close to the values adopted in our calculation ($\kappa = 0.125$, $R_b = 40$). Again we see qualitatively valid predictions by a linear theory in nonlinear flow situations. Besides, they assumed that wall effects act only on the longitudinal velocity and neglected any transverse force due to the wall. The observed systematic off-centre deviation was attributed to either experimental error or the

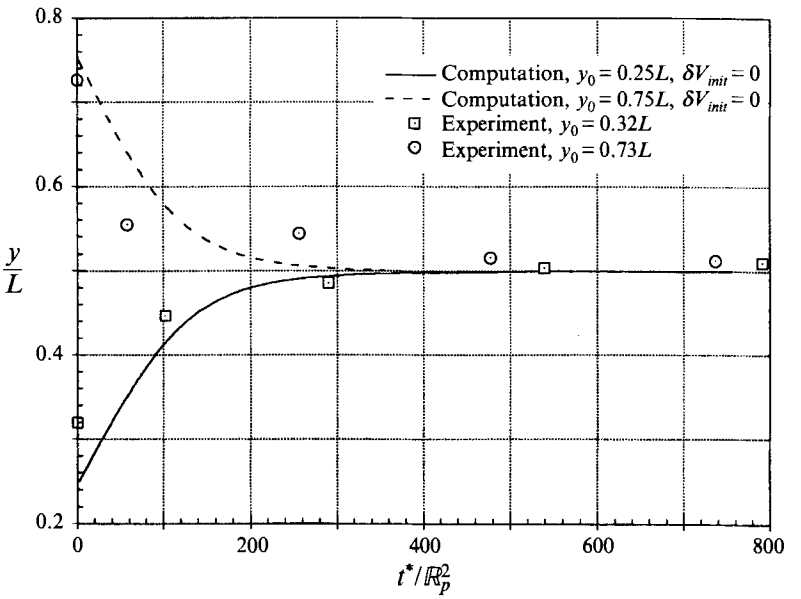

FIGURE 5. Particle trajectories predicted in our simulation compared to those observed by Halow & Wills (1970*b*) in a cylindrical Couette device. In the computation, $R_p = 0.625$, $\kappa = 0.125$. In the experiment, $R_p = 1.601$, $\kappa = 0.179$.

curvature of the velocity profile. Ho & Leal (1974) later managed to incorporate the curvature of the velocity profile in their theory and claimed to have successfully predicted the off-centre equilibrium position, although the parameters in the experiment are much larger than the $\kappa \ll 1$ and $R_p \ll \kappa^2$ assumed by their perturbation theory.

Despite the general agreement among experiments, theories and direct simulations, the physical mechanisms of the lateral migration are unknown till this point. Three factors are possibly responsible for the migration. The first is the wall repulsion, which is a lubrication effect known to force a sedimenting particle away from a nearby wall to the centre of the channel (Feng *et al.* 1994). In the present case, the relative motion of the particle to the nearby wall induces this repulsion that makes the centre an equilibrium. Another possible mechanism is proposed based on a perturbation result. Bretherton (1962*a*) and Saffman (1965) showed that a particle will move into the slower stream of a shear flow if the slip velocity is such that the particle leads the fluid and will move into the faster stream if the particle lags the fluid. In our simulation, a lead velocity is obtained for all runs, which suggests a lift force similar to the Bretherton–Saffman lift (see (1.1) and (1.2)) towards the centre. We emphasize that the fluid mechanics of this lift (termed inertial lift hereafter) may be vastly different from the viscous perturbation lift. The last possible cause of the migration is a Magnus type of lift associated with the rotation of the particle. The counterclockwise rotation of the particle, together with the lead velocity, may produce a lift force that points from both walls to the centre of the channel (Rubinow & Keller 1961). Next, we will verify or dismiss the three mechanisms proposed by examining the distribution of the pressure and shear stress on the surface of the particle. We note that the viscous normal stress $\sigma = 2\mu\,\partial u_r/\partial r$ is identically zero on the surface.

Figures 6 and 7 show the distribution of the pressure and the shear stress on the surface of the circular particle at an early time when the lateral drift is substantial and

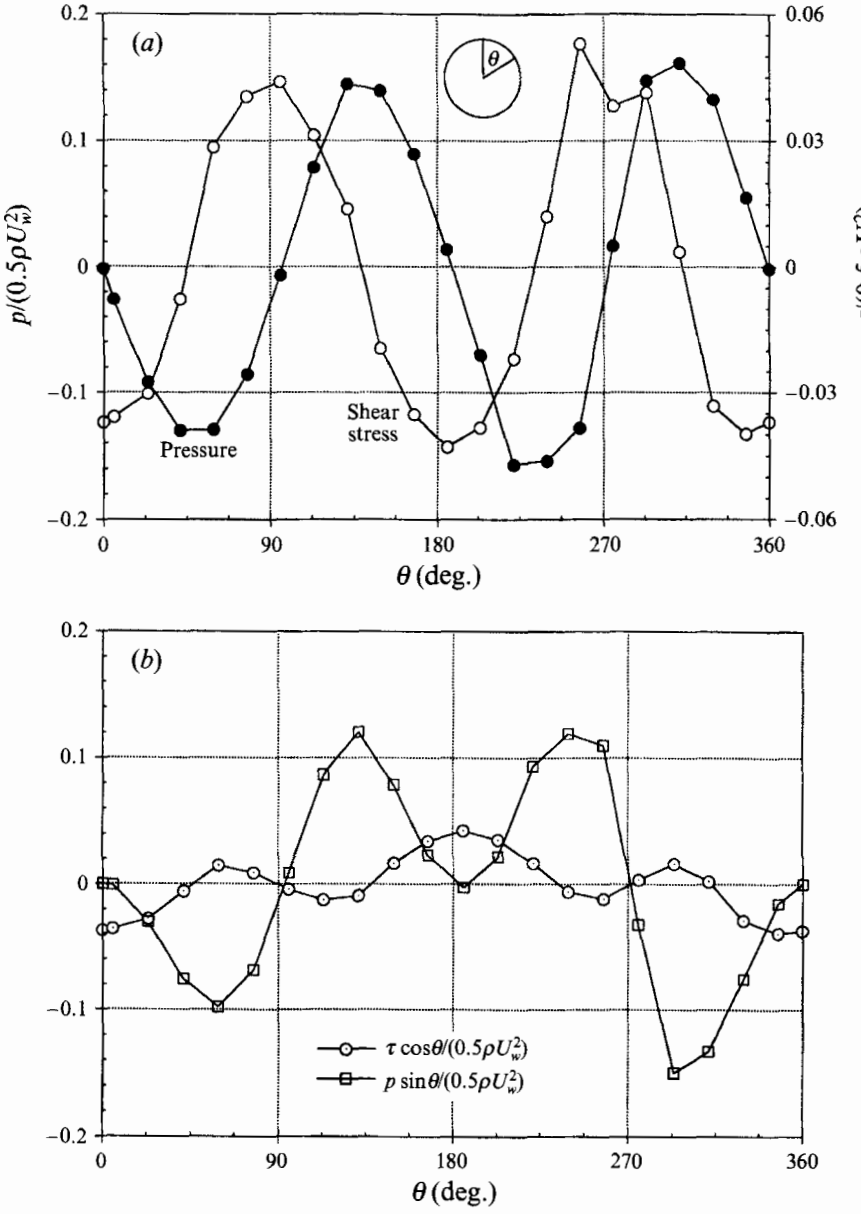

FIGURE 6. Distribution of pressure and viscous stresses on the surface of the particle at an early time of migration (curve 1 in figure 2). $t^* = 1.479$, $(x, y) = (0.2895L, 0.25275L)$. (*a*) Pressure and shear stress; (*b*) horizontal projections. Because of the definition of the angle θ, negative projection corresponds to lateral lift in the positive y-direction (to the right). The resultant lateral thrusts per unit length (scaled by the inertial force $\rho U_w^2 a$) are: $F_p = 7.842 \times 10^{-3}$, $F_\tau = 5.238 \times 10^{-3}$.

at a later time when the particle migration has stopped on the centreline of the channel. Because pressure usually plays the most important role in determining the particle motion (Huang *et al.* 1994; Liu *et al.* 1993), we will study the pressure distributions first.

We first notice that for both times the pressure distribution has two maxima and two minima on the surface. This is because the relative flow seen by the particle comes onto

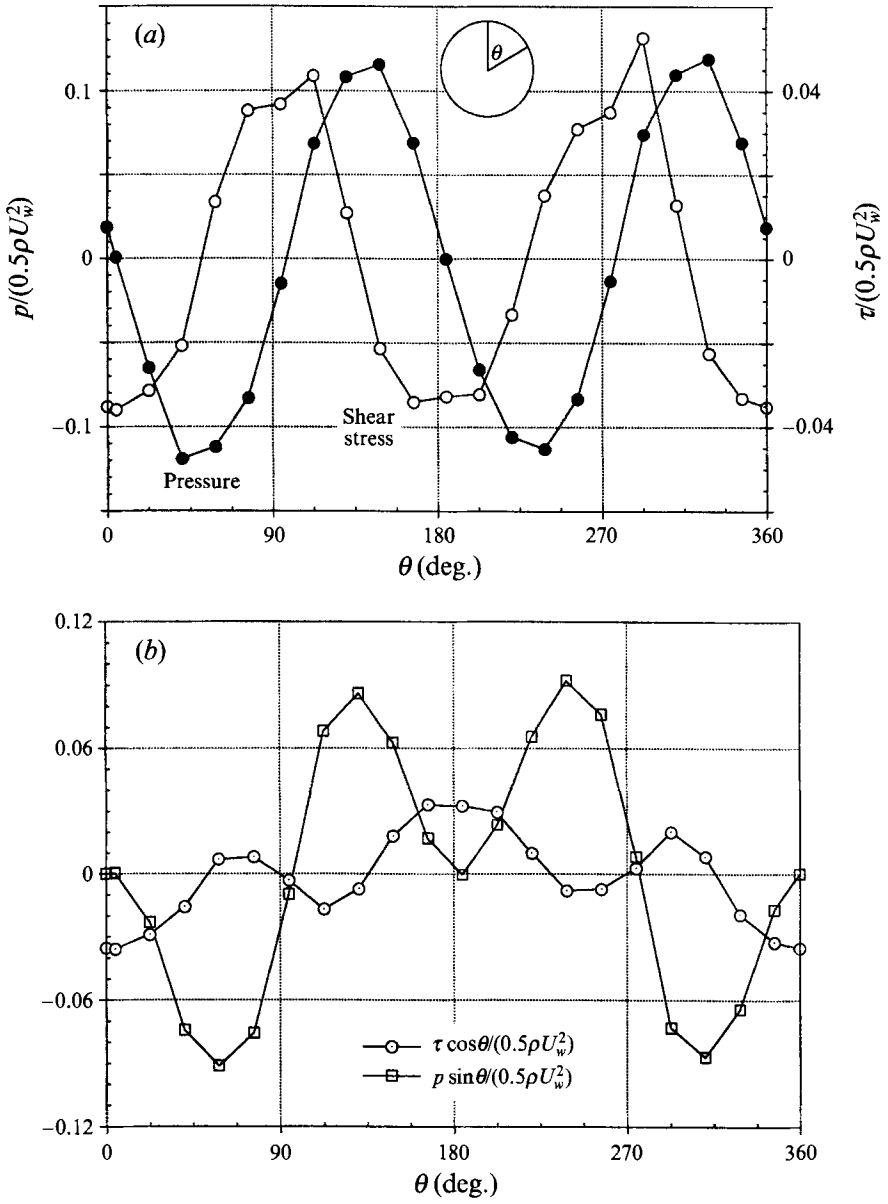

FIGURE 7. Distribution of pressure and viscous stresses on the surface of the particle at a late time of migration (curve 1 in figure 2). $t^* = 176.5$, $(x, y) = (8.53L, 0.49825L)$. (*a*) Pressure and shear stress; (*b*) horizontal projections. Because of the definition of the angle θ, negative projection corresponds to a lateral lift in the positive y-direction (to the right). The dimensionless resultant lateral thrusts are: $F_p = -1.558 \times 10^{-3}$, $F_\tau = 9.446 \times 10^{-4}$.

its left and right sides in opposite directions. We call attention to the fact, already noted by Huang *et al.* (1994) and Liu *et al.* (1993), that the pressure extrema correspond more or less to the zeros of the shear stress. This correspondence would be even stronger if the negative shear stress due to the slow rotation of the particle were taken away (see Liu *et al.* 1993). Because the particle is rotating in a viscous fluid with closed streamlines around it (Cox *et al.* 1968), stagnation points cannot be strictly defined on the surface of the body. But we will still call points with maximum or minimum

pressure 'viscous stagnation points'. It is probable that the stagnation points with negative pressures evolve into points of separation.

In figure 7(*a*), the pressure distribution has a symmetric pattern and the lateral thrust cancels out between the first and the second quadrant, and between the third and the fourth (figure 7*b*). This is of course understandable as the particle has reached the centreline at this stage. In contrast, the pressure distribution in figure 6(*a*) displays apparent asymmetry. On the left side of the particle, the maximum pressure (at $\theta = 311°$ is higher than its counterpart on the right side (at $\theta = 131°$), and the minimum pressure (at $\theta = 221°$) is lower than its counterpart (at $\theta = 41°$). Considering the position of the particle, this asymmetry can be evidently attributed to the wall effect. The highest pressure in the fourth quadrant arises as the wall, which is moving down faster than the particle, forces fluid through the gap (see figure 1). This effect is known as lubrication if the gap is very narrow, and as geometric blocking otherwise. We will loosely call this a lubrication effect for any gap size.

The average high pressure in the second quadrant nearly balances the average low pressure in the first quadrant, but the average high pressure in the fourth is not compensated by the negative pressure in the third quadrant. This leads to a net lateral thrust to the right toward the centre of the channel. The horizontal projection of the pressure in figure 6(*b*), which gives the lateral thrust directly, shows this imbalance more clearly. We also note that because of the lubrication effect on the left side of the particle, the average pressure on the top of the particle is larger than the average pressure on the bottom, producing a positive slip velocity with which the particle leads the fluid. The same argument holds for a particle initially on the right side of the channel. The above analysis establishes the wall lubrication as the dominant mechanism for the migration of a neutrally buoyant particle in a Couette flow.

We now turn our attention to the inertial lift related to shear and slip. The downward lead velocity of the particle in the left half of the channel tends to enhance the upward flow on the right side of the particle and suppress the downward flow on its left. However this mechanism affects the pressure distribution and the transverse force, it is small in magnitude and is overshadowed by the strong wall effect in figure 6. An indication of its existence can be found, however, in the initial transient of curve 4 in figure 4. For a brief moment after the release, the particle has a large negative slip. This produces a short-lived migration toward the wall. After the slip velocity relaxes to a small positive value, this mechanism becomes much smaller and, because it is now in the same direction as the wall repulsion, no longer distinguishable. In the next section, the inertial lift will be fully revealed for non-neutrally buoyant particles that have large slip velocities.

The rotation of the particle may be the reason for the shift of the pressure distribution in figure 7(*a*). Because the slip velocity is very small, the contribution of rotation to the lateral lift is conceivably minimal. For non-neutrally buoyant particles, however, rotation will be a considerable element in the lateral migration (see §2.2).

Pressure differences do not only move the particle, they also move the fluid from high-pressure regions to low-pressure regions. The high pressure in the fourth quadrant, caused by lubrication, pushes the fluid from the fourth to the first quadrant. This flow gives rise to a shear stress on the top of the particle that drags it to the centre. An opposing and stronger shear appears on the bottom, and the net effect of the shear stress is to generate a small thrust to the left. As the particle approaches the centreline, the asymmetry in the stresses, produced mainly by lubrication, is relieved and the resultants due to pressure and shear stress tend to vanish (figure 7*b*).

Finally, it is impossible to identify the physical picture constructed above with either

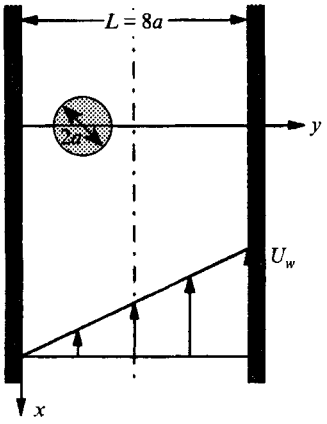

FIGURE 8. Migration of a buoyant particle in an upward Couette flow between walls.

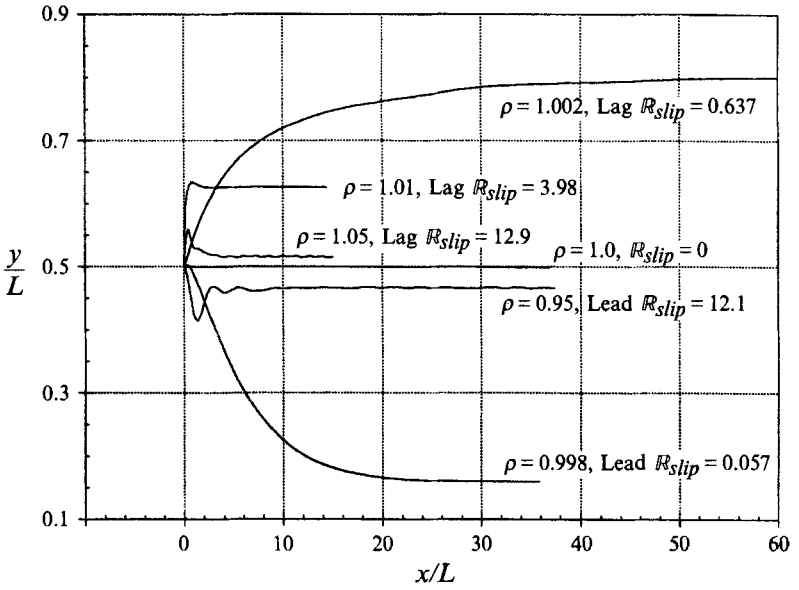

FIGURE 9. The migration of buoyant particles released at $y_0 = \frac{1}{2}L$ in a Couette flow field. The moving wall is at $y = L$. The slip Reynolds number is defined by $R_{slip} = 2|\delta V|a/\nu$, so $|\delta V|U_w = 0.1\ R_{slip}$. Since the heaviest particle is falling down, positive x has been used for all cases.

the Bretherton–Saffman viscous perturbation theory or the inertial perturbation theories of Ho & Leal (1974) and Vasseur & Cox (1976). These theories are only weakly nonlinear and they leave out important physical mechanisms like lubrication effects which arise when a particle of finite size approaches a wall.

2.2. *Non-neutrally buoyant particles*

The buoyant weight of the particle defines a slip velocity that can be either upward or downward, depending on the density of the particle. To be definite about the flow directions, we now consider the upward Couette flow shown in figure 8, in which $\kappa = 0.125$, $R_b = 40$ and $Fr = 392$.

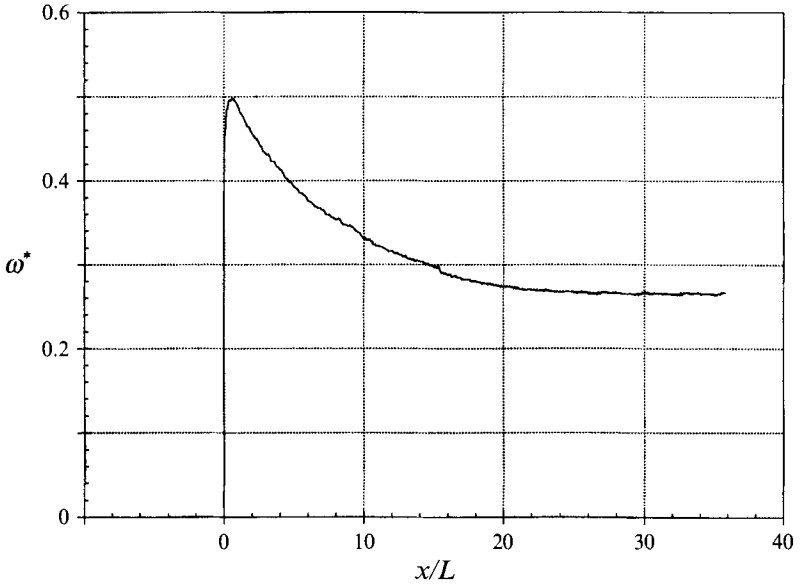

FIGURE 10. The angular velocity (made dimensionless by the shear-rate $\omega^* = \omega L/U_w$) of a slightly buoyant particle decreases as it approaches the wall. $\rho = 0.998$, final lead $\mathcal{R}_{slip} = 0.057$.

Numerical simulations of the motion of particles of various densities have been carried out. Some of the results are shown in figure 9. If the particle is only slightly buoyant ($\rho = 0.998$ or 1.002), it stabilizes at a position close to either of the walls, depending on whether it leads or lags the fluid; a light particle ends up close to the stationary left wall and a heavier one close to the moving right wall. For larger buoyancy ($\rho = 0.95$, 1.01 and 1.05), however, the final position of equilibrium moves back toward the centreline. These results can be interpreted in the light of the mutual action of the three fluid mechanical agents proposed in the last section, namely the wall repulsion, the inertial lift and the rotation-related lift.

Note that even the smallest buoyancy tested here causes a slip velocity much larger than that of a neutrally buoyant particle (figure 3). For instance, at $x = 2a$, the particle with $\rho = 0.998$ has a lead velocity of $0.018U_w$. This will boost the inertial lift and the lift caused by particle rotation, which force leading particles to the stationary wall and lagging ones to the moving wall. Later in this section we will illustrate the physical mechanism of the inertial lift by studying the distributions of pressure and shear stress on the particle surface. The particle cannot go all the way onto the wall because of the wall repulsion, and it will stabilize at a stand-off distance from one of the walls where the lubrication force from the wall cancels the inertial lift and the lift due to rotation. Another effect of the wall is to suppress the rotation of the circular particle (*figure 10*).

If the difference in density is increased, the slip velocity gets even larger. The motion of the particle becomes dominated by the slip velocity as in sedimentation. The wall lubrication force will be greatly increased. The inertial lift, however, will be increased much less than the wall repulsion. This can be understood by realizing that the difference in velocity across the particle caused by shear is less important when the slip is large (cf. figure 12*c*). We note that McLaughlin (1991), by extending the Saffman perturbation to allow strong slip, proved that the Saffman lift force even decreases when the slip velocity is large enough. This seems to be consistent with our argument although a decrease in inertial lift has not been shown in our simulations. Finally, our

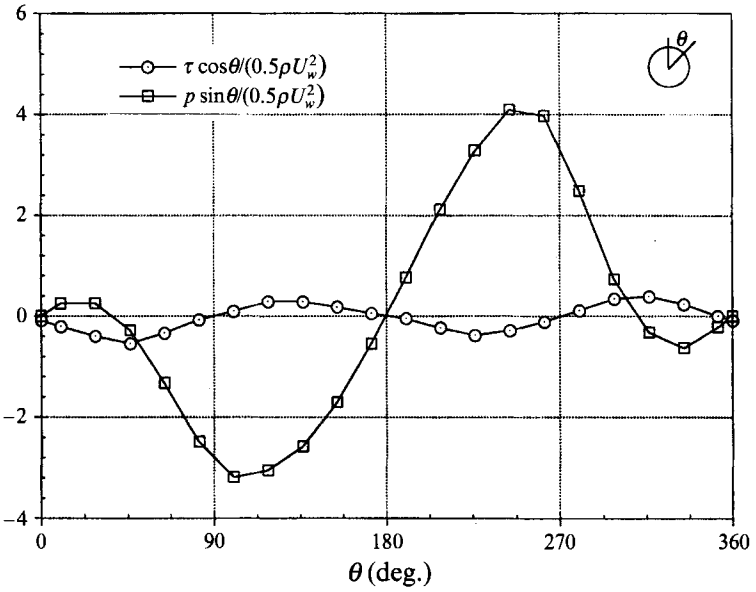

FIGURE 11. The horizontal component of pressure and shear stress at an early stage of migration of a lighter particle ($\rho = 0.95$). $(x, y) = (0.3427L, 0.4865L)$. Because of the definition of θ, a positive lateral thrust corresponds to a lift in the negative y-direction. The dimensionless resultant forces are $F_p = -0.2586$, $F_\tau = 0.1001$.

results show that the rotation is much suppressed by the strong slip. The final angular velocity of particles of density $\rho = (0.95, 0.998, 1.0, 1.002, 1.01, 1.05)$ is $\omega^* = (0.21, 0.265, 0.472, 0.476, 0.229, 0.184)$. The above arguments explain why particles of great buoyancy, whether lighter or heavier, assume equilibrium trajectories closer to the centre of the channel.

The driving forces of the migration have their origins in the pressure and the shear stress on the surface. As indicated in §2.1, the pressure distribution determines the qualitative pattern of migration and the viscous shear stress only has relatively minor influences. This is further illustrated by a typical case shown in figure 11. The following analysis focuses on the mechanisms by which the flow field around the particle dictates a particular pressure distribution which gives rise to the inertial lift and wall repulsion. The effect of rotation will be examined separately. Without losing generality, we will consider lighter particles only. Early and final stages of migration are investigated, when the particle is on the centreline or closer to a wall. This allows us to study the inertial lift and wall repulsion separately.

When the density difference is small, the particle sees flow coming to its left and right sides in opposite directions (figure 12*a*, *b*). This gives rise to a pair of pressure extrema on each side of the particle (figure 13*a*, *b*). We again note that the location of the extrema of pressure p corresponds roughly to points of vanishing shear stress τ. Since the particle leads the local fluid in this particular example, the flow is stronger on its left flank where the maximum pressure is larger and minimum smaller. At the beginning of the migration, when the particle is near the centreline (figures 12*a* and 13*a*), careful comparison shows that the mean pressure is actually lower on the left, which is reminiscent of potential flow around a rotating cylinder. It is not the front stagnation pressure around $\theta = 320°$ that determines the migration. Instead, it is the negative rear stagnation pressure at $\theta = 225°$ that gives rise to the dominant inertial lift

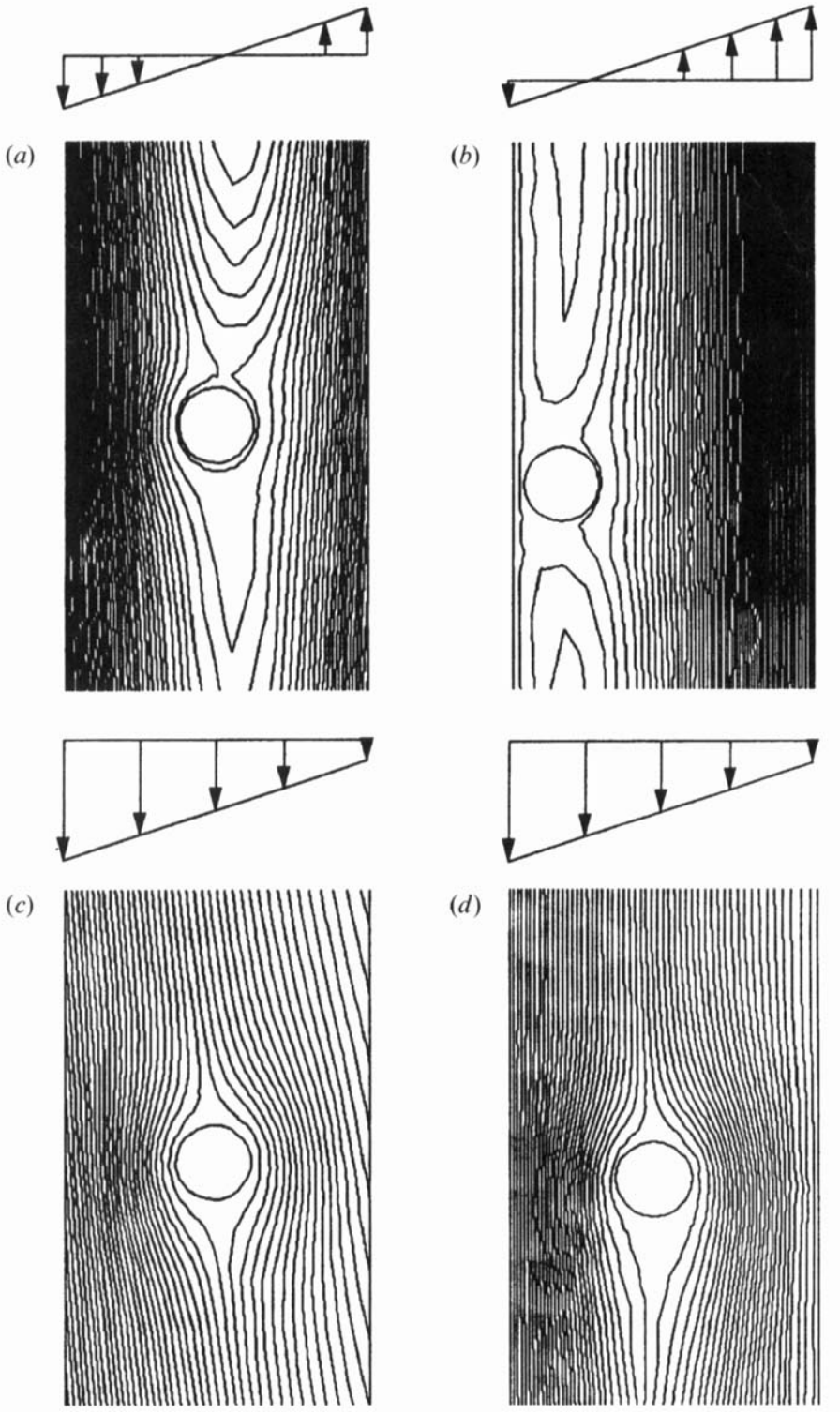

FIGURE 12. Streamlines around a buoyant particle as seen in a coordinate system fixed on the particle. The four cases represent the early and final stages of migration of a particle with small and large slip velocities. The sketch shows the undisturbed relative velocity for each case. (*a*) $\rho = 0.998$, $(x, y) = (0.8078L, 0.4995L)$; (*b*) $\rho = 0.998$, $(x, y) = (35.85L, 0.16L)$; (*c*) $\rho = 0.95$, $(x, y) = (0.3427L, 0.4865L)$; (*d*) $\rho = 0.95$, $(x, y) = (46.80L, 0.4655L)$.

that moves the body toward the left wall. At the final stage of migration (figure 12*b*), the proximity of the wall has two effects on the pressure distribution. First, the magnitude of both pressure extrema is increased, and they are closer together. The other effect is that the mean pressure on the left is increased to balance the inertial lift (figure 13*b*). This wall repulsion reflects the lubrication effect between the wall and the particle, and is basically the same mechanism that forces a neutrally buoyant particle to the centreline as demonstrated in the last subsection.

If the density difference is large, the flow field resembles that caused by a sedimenting particle, and the effect of shear and particle rotation is not conspicuous in the streamlines (figure 12*c*, *d*). The pressure distribution is similar to that on a sedimenting particle as well, only the difference in the 'intensity' of the flow on both sides distorting the symmetry to produce a higher average pressure on the right side of the particle (figure 13*c*). We note again that the negative pressure at the back of the particle determines the direction of migration. It is interesting that in low-Reynolds-number sedimentation near a wall, it is the front stagnation pressure that makes the major contribution to lateral motions (Liu *et al.* 1993). At the later stage of migration, the wall effect negates the inertial lift and forces the particle back to an equilibrium position near the centreline (figure 13*d*).

If one ignores the details of pressure distribution, the inertial lift described above can be likened to the lift on an airfoil, where faster flow induces lower pressure on one side of the body than on the other side. But here the asymmetry in flow intensity arises mainly as a result of shear and slip velocity. The effect of particle rotation, which corresponds to the circulation around an airfoil, will be addressed next in this section. If there is no slip velocity, the shear flow will be skew-symmetric between the two sides of the body. If there is no shear, the flow induced by a settling particle is symmetric. In both cases, there is no difference in the intensity of flow on both sides of the particle, and no inertial lift could exist. This reveals the mechanism of the inertial lift. This argument also suggests that very large slip velocity will suppress the inertial lift as already mentioned.

To study the effect of rotation, we computed the migration of buoyant particles prevented from rotation, and the trajectories are shown in figure 14. Non-rotating particles always assume an equilibrium position somewhat closer to the centreline of the channel, so they experience a smaller transverse force toward the wall although the slip velocity is slightly larger. This suggests that the lift due to rotation plays a small but definite role in the lateral migration, and it is in the same direction as the lift caused by shear slip. This is a nonlinear effect, and has not been included in the lift forces of Bretherton (1962*a*) and Saffman (1965). The rotation effect has other implications for the migration behaviour. In particular, a particle with large slip velocity has small rotation, and this helps to explain the reversal in the shift of equilibrium position as the slip velocity increases (figure 9). Microscopically, rotation influences the layer of fluid that adheres to the surface, and alters the distribution of shear stress and pressure.

In summary, we may say that the inertial lift is mainly caused by the difference in the intensity of flow between the two sides of the particle due to shear slip. Particle rotation contributes to the migration by inducing a lift of relatively small magnitude. The wall repulsion is a lubrication effect. Another effect of the wall is that it tends to suppress the rotation and thus diminish the lift due to rotation.

As far as we know, Vasseur & Cox (1976) is the only study, theoretical or experimental, that addresses the migration of buoyant particles. In the limit of small particles and vanishing Reynolds numbers, their analysis shows that in a Couette flow, if the particle leads the fluid (a lighter particle in upward flow or a heavier particle in

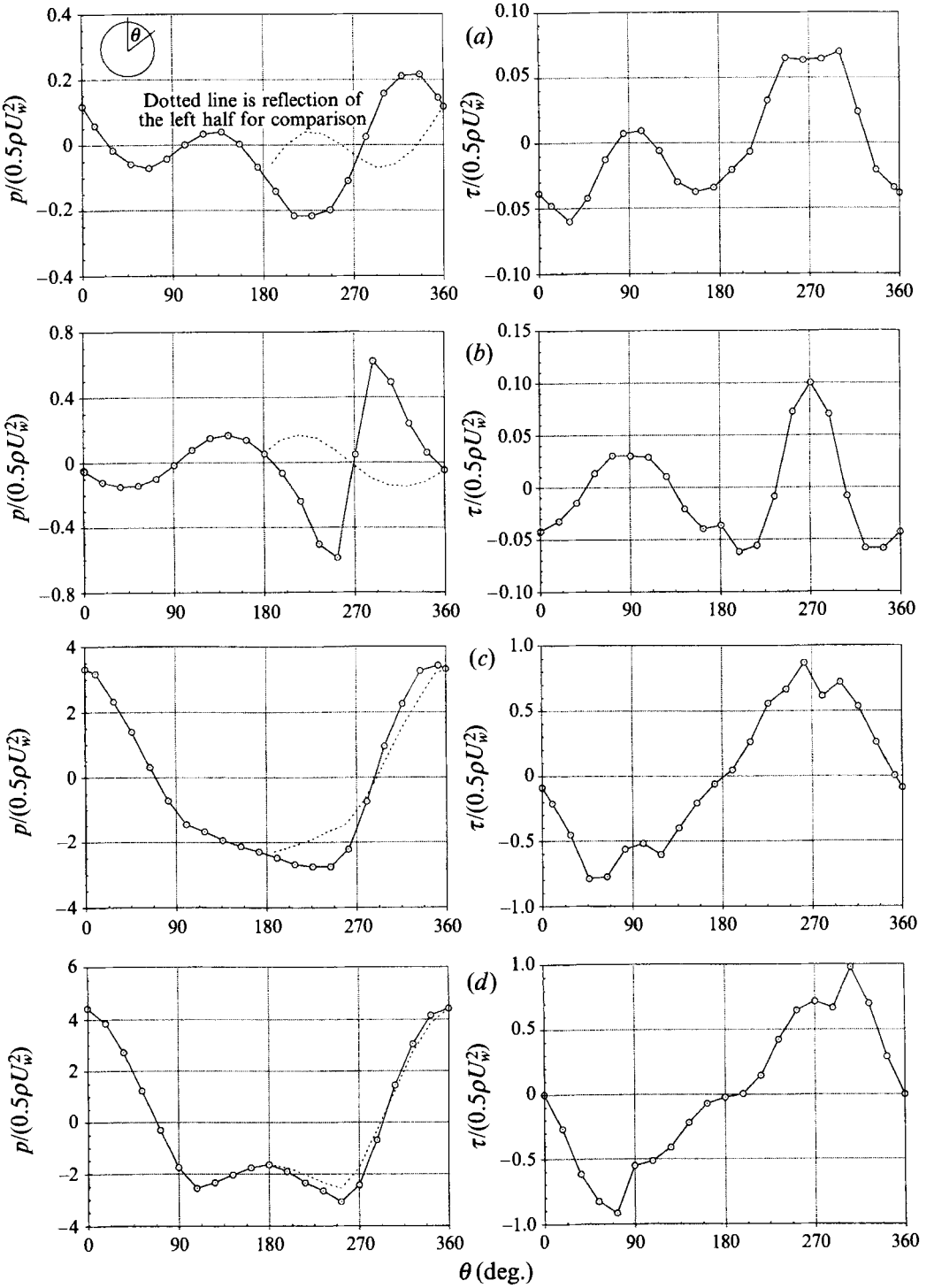

FIGURE 13. The pressure and shear stress distributions on a buoyant particle in a Couette flow. The four cases (a, b, c, d) are the same as shown in figure 12.

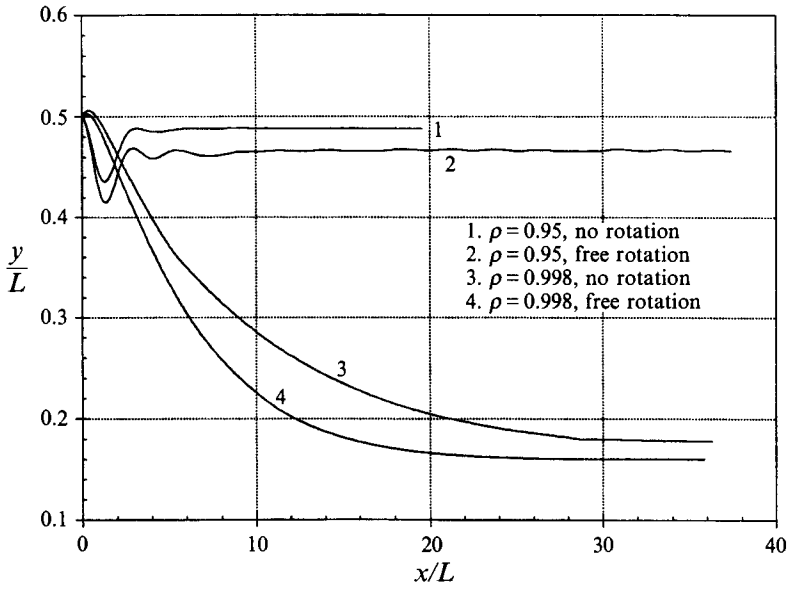

FIGURE 14. The migration of freely rotating and non-rotating buoyant particles.

downward flow), it migrates to the stationary wall; a lagging particle goes to the moving wall. The direction of migration agrees with our two-dimensional simulations for small buoyancy. However, the perturbation theory does not predict the stand-off distance from the wall in the final trajectory and the migration of particles with large buoyancy.

3. Particle migration in a planar Poiseuille flow

Particle motion in a Poiseuille flow is of more engineering interest than that in a Couette flow. On the theoretical side, the problem has been studied by perturbations. Under the small-particle and low-Reynolds-number restrictions, Ho & Leal (1974) predicted a Segré–Silberberg effect for neutrally buoyant particles. Vasseur & Cox (1976) later obtained similar results using an alternative approach, and further studied the case of non-neutrally buoyant particles. Their major conclusion is that a particle leading the fluid will migrate to the wall while one lagging migrates to the centreline. We have relaxed the restrictions to small particles and low Reynolds number in our simulations, as for the Couette flow, and find that leading particles are repelled near the wall at an equilibrium stand-away distance and that lagging particles never get to the centreline at any finite fluid speed but attain an equilibrium close to the centreline, whose exact position also involves the effects of the wall. We shall present and interpret the results of our simulations for neutrally buoyant and non-neutrally buoyant particles and compare them with previously published theoretical and experimental data.

3.1. *Neutrally buoyant particles*

The channel and the particle are the same as used in the Couette flow, except that the characteristic velocity of the undisturbed flow is now the maximum velocity at the centre of the channel U_m (figure 15). Shown in figure 16 are the migration curves for neutrally buoyant particles released at different initial positions. The Segré–Silberberg effect is realized, with the equilibrium position a little outside the midpoint between the

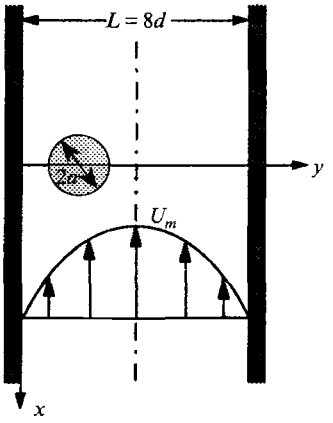

FIGURE 15. Geometry for the migration of a particle in a plane Poiseuille flow.

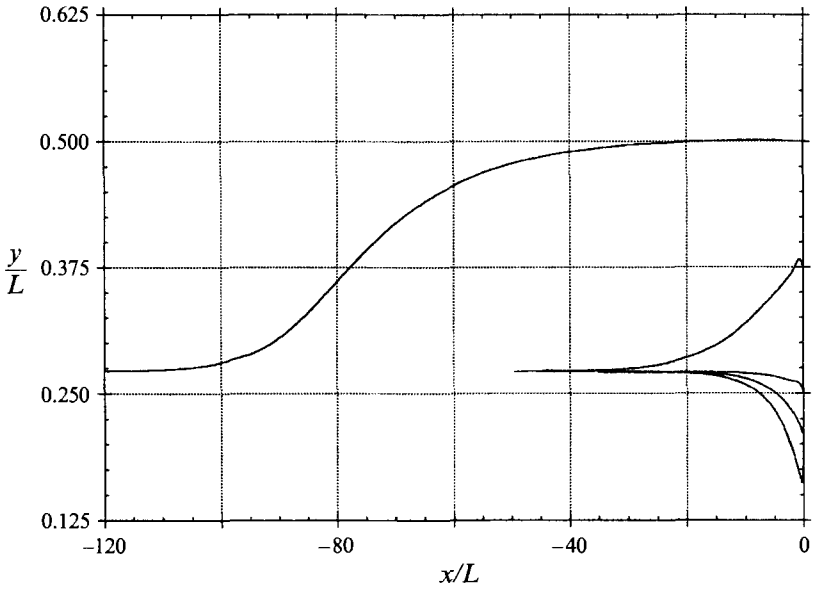

FIGURE 16. The Segré–Silberberg effect in a plane Poiseuille flow field. Particle Reynolds number $\mathcal{R}_p = 0.625$; bulk Reynolds number $\mathcal{R}_b = 40$.

wall and the centre at $y = 0.252L$ when the particle Reynolds number $\mathcal{R}_p = 0.625$. If we increase the velocity at the centre of the channel, the particle migrates faster and the final equilibrium position is closer to the wall (figure 17).

The symmetry of the Poiseuille flow field makes the centreline of the channel an equilibrium position for a circular particle; but it is not a stable one. If the particle is displaced slightly to the left, hydrodynamic forces will develop which push the particle further to the left (the same argument works on the right side). The destabilizing mechanism is associated with the curvature in the undisturbed velocity profile, as we will proceed to show next.

First we note that the particle always lags the local velocity of the undisturbed flow.

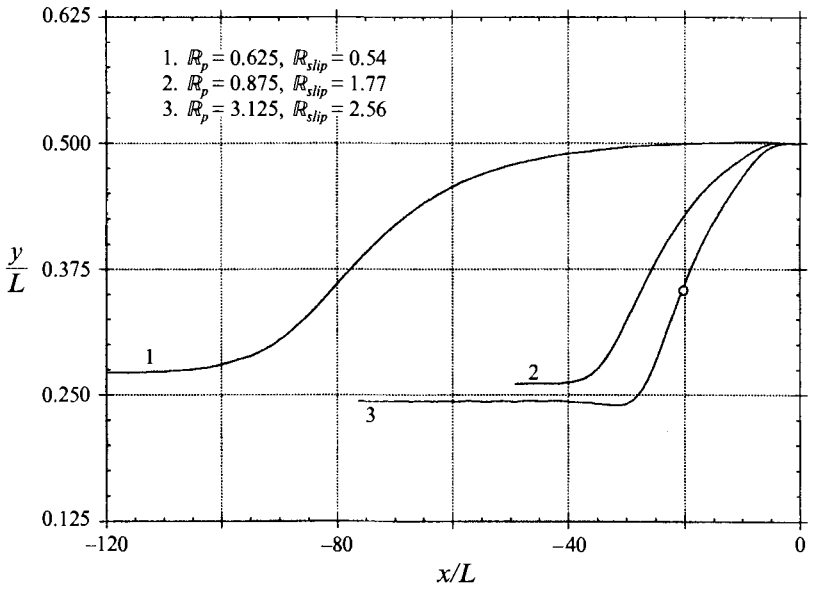

FIGURE 17. The effect of the flow rate on the Segré–Silberberg migration. The circle on curve 3 marks the position at which the flow around the particle is analysed in figures 19 and 20.

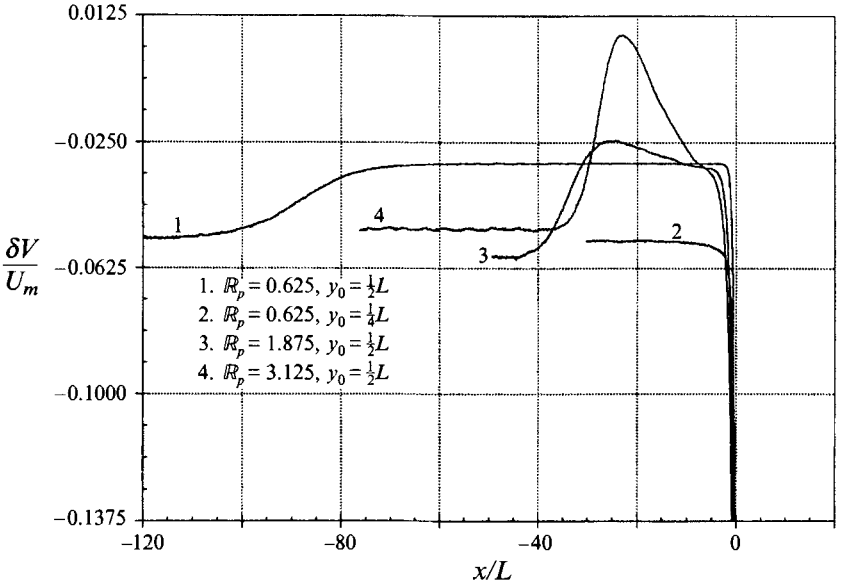

FIGURE 18. The slip velocity of particles released from different positions in the flow at different apparent Reynolds numbers.

This is a well-known effect in the limit of small particles in slow flows (Brenner 1966) and is here shown to be general. In figure 18, we compare the lagging velocities for different flower rates. For a fixed U_m, the slip velocity rapidly relaxes to a constant value independent of the initial conditions, although the rate of relaxation may be different. At higher U_m, the slip velocity δV is larger.

If the curvature of the velocity profile were zero, the negative slip velocity would

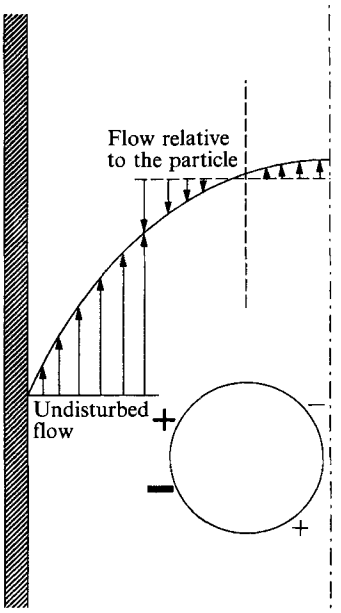

FIGURE 19. Cartoon showing the relative flow and pressure extrema around a neutrally buoyant particle in a Poiseuille flow. The particle is in a position marked in figure 17. $R_p = 3.125$.

cause a stronger relative flow on the right of a particle which is in the left side of the channel. Then the average pressure would be lower on the right and the particle would be pushed to the centre of the channel. The curvature reverses this trend as shown in figure 19. At this particular time step, the velocity of the particle is $0.903U_m$, and the undisturbed fluid velocity is $0.925U_m$ at the centre of the particle, $0.725U_m$ at its left tip and $0.999U_m$ its right tip. It is clear that the curvature creates a higher velocity of the fluid relative to the particle on the left side. The effect overwhelms the asymmetry caused by the lag velocity. By the same argument given for a non-neutrally buoyant particle in a Couette flow, the stronger flow causes low pressure on the left side of the particle and sucks it away from the centreline. This mechanism can be further illustrated by the distributions of pressure and shear stress on the surface of the particle (figure 20).

As in the case of a neutrally buoyant particle in a Couette flow, there are four distinguished points on the boundary of the circular particle corresponding to zeros of the shear stress (figure 20). The two extrema on the right side of the particle are relatively weak. The highest pressure occurs at the 'stagnation point' in the fourth quadrant ($\theta = 308°$) on the left, and is marked by a thick plus symbol in figure 19. But the negative pressure at $\theta = 236°$ is even larger in magnitude and is marked by a thicker minus. This negative pressure gives rise to a lateral thrust that points toward the left wall (figure 20*b*). It can also be seen that the stronger relative flow on the left of the particle is reflected by larger shear stress there (figure 20*a*).

Owing to the small magnitude of the slip velocity, the inertial lift caused by shear slip and the lift related to particle rotation are believed to be small. The lateral drift of the particle stops when the lubrication effects arising from the wall force equilibration of all the lateral thrust forces.

The effect of curvature in the Poiseuille velocity profile was first pointed out by Ho & Leal (1974) in their perturbation theory. The physical picture given here, however, could not possibly be constructed by the asymptotic analysis. Our numerical simulation

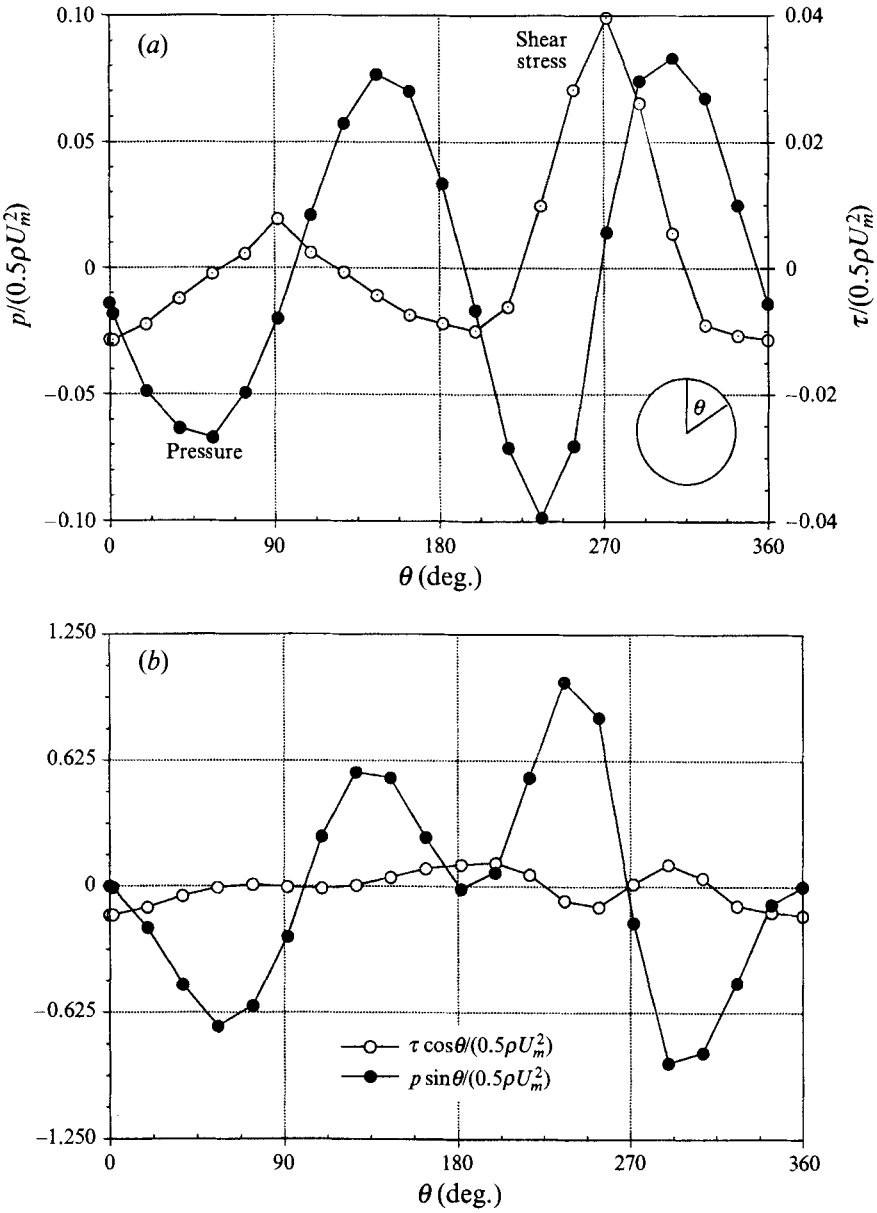

FIGURE 20. Distributions of pressure and viscous stresses on the surface of a neutrally buoyant particle in a Poiseuille flow. $\mathcal{R}_p = 3.125$. The position of the particle is $(x, y) = (19.82, 0.3628)$ L, which is marked by a circle in figure 17. (*a*) Pressure and shear stress; (*b*) horizontal projections. Because of the definition of θ, positive projection corresponds to lateral thrust toward the left wall. The resultant lateral forces (scaled by the inertial force $\rho U_m^2 a$) are: $F_p = -3.67 \times 10^{-3}$, $F_\tau = -6.725 \times 10^{-4}$.

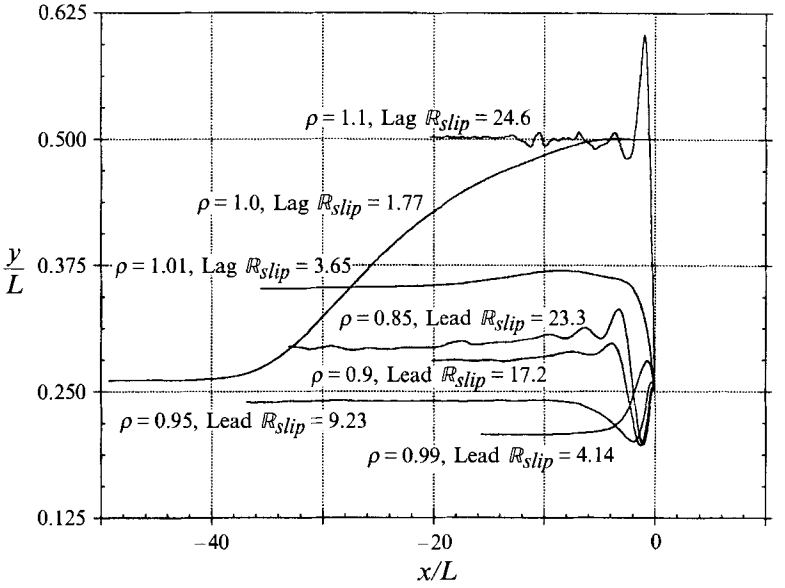

FIGURE 21. The migration of buoyant particles in a plane Poiseuille flow. $R_b = 120$, $R_p = 1.875$, $F_r = 43.56$. Initial position $y_0 = \frac{1}{4}L$ except for the neutrally buoyant case shown here for comparison.

for large particles ($\kappa = 0.125$) at moderate Reynolds numbers ($R_p \sim 1$) agrees qualitatively with the perturbation theories, although the equilibrium position predicted here ($\sim 0.25L$) is closer to the centreline than in the theories ($\sim 0.2L$).

3.2. *Non-neutrally buoyant particles*

Particles of various densities, either larger or smaller than that of the carrying fluid, are released halfway between the wall and the centre. The migration curves are shown in figure 21. A neutrally buoyant particle released at the centreline is also shown for comparison.

These trajectories can be interpreted based on the understanding of the migration of a buoyant particle in a Couette flow and the effect of velocity profile curvature. As discussed previously, a neutrally buoyant particle in a Poiseuille flow lags the fluid slightly, and the wall effect balances the effect of the curvature of the velocity profile, giving rise to an equilibrium position about halfway between the centre and the wall. If the particle is slightly heavier than the fluid, the lagging velocity is larger, resulting in a larger inertial lift that moves the particle closer to the centre ($\rho = 1.01$). At even larger density difference and larger lag velocity, the inertial lift and the wall effect are dominant so that the particle is pushed to the centre rapidly, overshooting and finally stabilizing at a position very close to the centreline ($\rho = 1.1$). Because of the curvature in the undisturbed velocity profile, the particle cannot stabilize exactly on the centreline.

If the particle density is only slightly smaller than that of the fluid, the slip velocity will be moderately leading. The inertial lift will point to the nearer wall and help the curvature effect to move the particle outward against the wall repulsion. The equilibrium position will then be closer to the wall ($\rho = 0.99$). If the density difference is sufficiently large, however, a reversal similar to the Couette case occurs. The slip velocity overshadows the effect of the Poiseuille velocity profile, and the motion of the

particle resembles sedimentation. Then the wall lubrication force overwhelms the inertial lift and the curvature effect, and the particle starts to move back to the centre. There should be a critical density difference for each flow rate that puts the particle closest to the wall. But in principle, the particle can never really get to the wall.

The perturbation theory of Vasseur & Cox (1976) has some interesting results for non-neutrally buoyant spherical particles that can be compared to our two-dimensional simulations. They first obtained solutions for three limiting cases:

(i) A buoyant particle in a quiescent or slow-moving fluid with $|V/U_m| \gg 1$, where V is the terminal velocity of the particle when settling in an unbounded domain, and U_m is the maximum velocity in the undisturbed flow. The particle is found to move away from the walls to an equilibrium position on the centreline of the channel.

(ii) A non-neutrally buoyant particle with $\kappa^2 \ll |V/U_m| \ll 1$. The particle moves to either the wall or the centreline depending on whether it leads or lags the fluid.

(iii) A neutrally buoyant particle with $|V/U_m| \ll \kappa^2$. The particle stabilizes at an equilibrium position between the centreline and the wall (Segré–Silberberg effect).

Case (i) involves the sedimentation of a particle, which was studied in Part I of this series (Feng *et al.* 1994). In the present case of sedimentation in Poiseuille flow, we find that the equilibrium tends to the centreline only asymptotically as $V/U_m \to \infty$. Case (iii) was discussed in §3.1 as associated with the result of Ho & Leal (1974). For case (ii), the conclusion drawn by Vasseur & Cox is apparently different from ours. Two intermediate cases that Vasseur & Cox studied as representing the conditions between the three limits are particularly relevant to our simulation:

(iv) The case intermediate between (ii) and (iii) with $|V/U_m| \sim \kappa^2$, when the particle is slightly buoyant (case *e* in their original paper). They found that the particle attains an equilibrium position between the centreline and the wall, and is close to the centreline if the particle lags but close to a wall if the particle leads, but never reaches the wall. This result is similar to our simulations of the migration of slightly buoyant particles ($\rho = 1.01$, and probably also $\rho = 0.99$).

(v) The case intermediate between (i) and (ii) with $|V/U_m| \sim 1$, when the particle has a large slip velocity (case *d* in their original paper). Vasseur & Cox showed that the equilibrium position of the particle always approaches the centreline as the slip velocity increases, whether leading or lagging. This can be compared to our runs with $\rho = 0.85$, 0.90, 0.95 and perhaps 0.99. The reversal in the position of equilibrium of a leading particle as the slip velocity increases has not been reported elsewhere.

It should be emphasized that the Vasseur–Cox theory applies only under conditions $Re \ll 1$, $\kappa \ll 1$ and $Re \ll \kappa$. Therefore, the qualitative agreement between intermediate caves (iv) and (v) and our simulations may be fortuitous. For example, the non-neutrally buoyant particles in case (ii) are in fact very slightly buoyant particles in our case, and their results are different from ours. But their case (iv), which is for even less buoyant particles, does seem to agree with our simulation. The intermediate cases have not received much attention in the literature and the conclusions of the perturbation theory for case (ii) have long been taken as universally true for buoyant particles. The confusion related to the behaviour of a buoyant particle will be further addressed in the next subsection.

3.3. *Comparison with experiments*

Let us first discuss the motion of neutrally buoyant particles. Following Segré & Silberberg's (1961) observation, voluminous experimental work on the same kind of problem has verified their principal conclusions. For example, neutrally buoyant particles stabilize midway between the centreline and the wall, closer to the wall for larger flow rates and closer to the centre for larger particles (Karnis, Goldsmith &

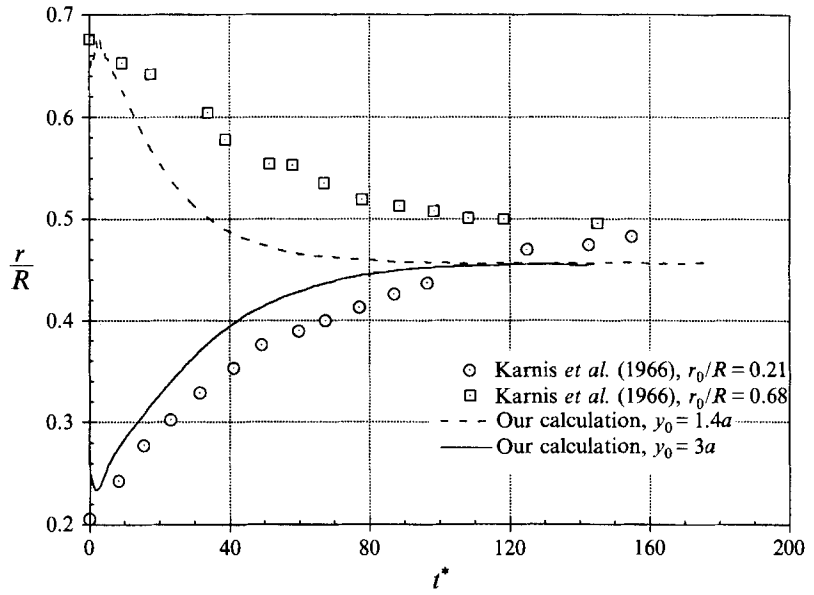

FIGURE 22. Comparison of the simulated Segré–Silberberg effect with the experiment of Karnis *et al.* (1966). The wall is at $r/R = 1$ or $y = 0$, and the centreline is at $r = 0$ or $y = 4a$. Other parameters are: Karnis *et al.*: $\mathcal{R}_{slip} = 7.4 \times 10^{-3}$, $\mathcal{R}_b = 26.4$, $a/R = 0.305$; our simulation: $\mathcal{R}_{slip} = 0.54$, $\mathcal{R}_b = 40$, $a/R = 0.25$.

Mason 1966). Because of the numerous parameters involved, however, attempts to establish a universal correlation have not been successful. This fact makes quantitative comparison among different studies difficult and less convincing. In our case, we also suffer from the geometric differences because most of the experiments used spherical particles in circular pipe flow. Nevertheless, it is interesting in a qualitative sense to see how the numerical prediction compares to the experimental data.

Karnis *et al.* (1966) presented extensive results on small particles, including spheres, rods and disks, migrating in a capillary tube. Because of the difference in particle Reynolds number $\mathcal{R}_p$, characteristic length and viscosity, the migration time differs from that of our simulation. We note that there are three major factors influencing the migration rate: the size of the particle, the inertia of the fluid and viscosity. The first effect was given as $(a/R)^2$ in their paper, where a and R are the radius of the sphere and the tube, respectively. To formulate the competition between the inertial and viscous effects, we simply use the ratio of the two:

$$t^* = \frac{\rho_f U_m^2}{\mu_f}\left(\frac{a}{R}\right)^2 t,$$

where U_m is the maximum velocity on the centreline. After this treatment, the typical inward and outward migration curves are compared in figure 22. Despite the difference in geometry, the behaviour of their sphere is very similar to that of our cylinder. The equilibrium position differs a little, but is closer to the centre than the wall in both studies. We remind the reader that owing to the complex nature of the problem, the timescale given above should not be expected to hold universally.

Tachibana (1973) conducted an experiment under conditions much more similar to our simulation in terms of dimension and geometry. His duct has a 3 cm × 3 cm square cross-section, producing two-dimensional Poiseuille flow fields at bulk Reynolds

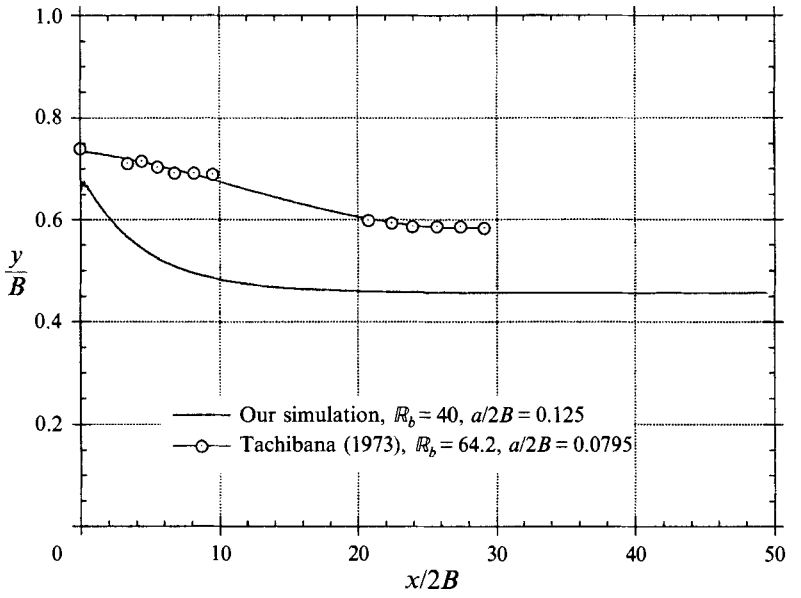

FIGURE 23. Comparison of the simulated migration trajectory of a neutrally buoyant particle with the experiment of Tachibana (1973). The width of the column is $2B$, and the centreline is at $y = 0$. The bulk Reynolds number is defined as $R_b = 2U_m B/\nu$.

number R_b (based on the size of the duct) up to 200. A typical inward migration trajectory is compared to our computation with the closest initial position in figure 23. Again, the simulation predicts qualitatively the same behaviour as observed in experiments.

As shown in figure 17, we have correctly simulated the effect of flow rate on the final equilibrium position. The influence of particle size is not systematically investigated in the computation. Based on the idea of competition among various lift forces, it is possible that larger particles induce larger lag velocities and therefore are pushed inward by stronger inertial lift and wall repulsion. In summary, our simulation of a neutrally buoyant two-dimensional particle migrating in a plane Poiseuille flow field does reproduce the major characteristics observed in three-dimensional experiments. Next, we will turn to the somewhat controversial non-neutrally buoyant case.

Review papers summarize the experimental findings by saying that leading particles migrate to the wall in a Poiseuille flow and lagging particles migrate to the centreline. This does not agree with our simulations. By investigating original experimental data, we will try to answer the following two questions:

(i) Does a lagging particle migrate to the centreline? Our computation suggests that the equilibrium position will be closer to the centreline as the density difference increases; at $R_{slip} = 24.6$, the particle stabilizes almost on the centreline (figure 21). In the experimental literature, most authors claim that a lagging particle goes to the centreline. This is true when the difference in density is large enough, which is the case in most of the experimental studies. However, the careful and comprehensive experiment of Repetti & Leonard (1966) in a plane Poiseuille flow does show that if the density difference is not large, the particle will stabilize at a small distance from the centreline. A similar conclusion was drawn by Aoki, Kurosaki & Anzai (1979) for a pipe flow. A detailed comparison will be given later in the section (figure 24). Based on our simulation and the experiments, as well as on the low-Reynolds-number asymptotic

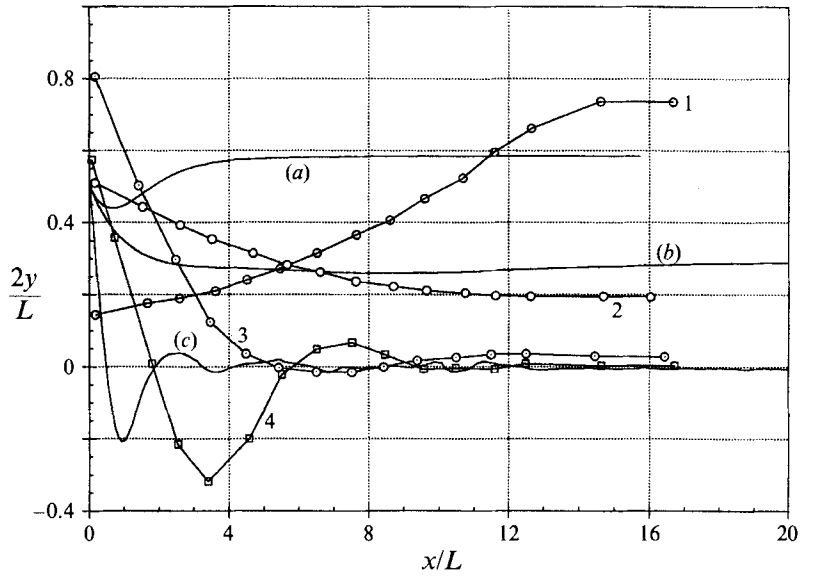

FIGURE 24. Migration of buoyant particles in a planar Poiseuille flow: comparison of our simulation with the experiment of Repetti & Leonard (1966). The centre is at $y = 0$ and the two walls are at $y = \pm\frac{1}{2}L$. Repetti & Leonard (downward flow): 1. $R_b = 412.3$, $\kappa = 0.0951$, $\delta\rho = 0.380\%$; 2. $R_b = 211.2$, $\kappa = 0.0473$, $\delta\rho = -0.091\%$; 3. $R_b = 408.5$, $\kappa = 0.0948$, $\delta\rho = -0.113\%$; 4. $R = 811.7$, $\kappa = 0.0951$, $\delta\rho = -0.322\%$. Our simulation (upward flow) at $R_b = 120$, $\kappa = 0.125$: (*a*) $\delta\rho = -1\%$, (*b*) $\delta\rho = 1\%$, (*c*) $\delta\rho = 10\%$.

analysis of Vasseur & Cox (case v in §3.2), we believe that the particle always assumes an equilibrium position between the centre and the wall. If the density difference is large enough, the particle will be very close to the centreline.

(ii) Does a leading particle migrate to the wall? In the literature we have found no experimental evidence of a particle going all the way to the wall. The earliest observations on density effects (Oliver 1962; Repetti & Leonard 1964; Karnis *et al.* 1966) indicated that particles leading the flow exhibit a two-way migration behaviour, depending upon their initial positions and/or density differences, very much in the same fashion that a neutrally buoyant particle migrates. The equilibrium position is near the wall, but a particle released next to the wall always drifts away due to wall repulsion. This is in perfect agreement with the results of our simulation (§3.2). The wall repulsion seems to have been overlooked by some later researchers, who, attempting to analyse the migration, have either considered the shear-related Saffman type of lift forces only (Denson, Christiansen & Salt 1966; Jeffery & Pearson 1965), or employed approximations that restricted the proximity of walls (Vasseur & Cox 1976). These analyses, claiming that leading particles go to the wall, were aggravated by improper extrapolations of experimental data which show that in a certain range of density difference, particles with larger lead velocity indeed attain equilibrium positions closer to the wall (Repetti & Leonard 1966). It is unfortunate that three widely cited review articles (Brenner 1966; Cox & Mason 1971; Leal 1980) have not given enough attention to the important two-way migration behaviour due to the complex competition among lateral forces.

A comparison between Repetti & Leonard's (1966) experimental data and our simulation will help to answer both of the above questions (figure 24). Working with a 2.54 cm × 10.16 cm rectangular cross-section duct, Repetti & Leonard created an essentially two-dimensional Poiseuille flow. In this figure, $y = 0$ is the centreline of the

channel and $y = \frac{1}{2}L$ is one of the two walls 2.54 cm apart. As our computation involves an upward flow while their flow is downward, opposite density differences correspond to the same particle–fluid slip condition in both studies. The density difference is represented by

$$\delta\rho = (\rho_{particle} - \rho_{fluid})/\rho_{fluid}$$

in the figure. For leading particles, their data (curve 1) agree qualitatively well with ours (curve *a*). It is clear that the particle is not able to travel all the way to the wall before being stopped by the wall repulsive lift (see also Karnis *et al.* 1966). For particles only slightly lagging the fluid, curve 2 verifies our conclusion that the particle does not go all the way to the centreline. Instead, it stops somewhere close to the centreline where the inward lift is balanced by the outward force related to the velocity profile curvature (*b*). At larger lagging velocity, the particle is even closer to the centreline (3). If the large velocity is still larger, inertia of both the particle and the fluid becomes so important that the particle oscillates a few times before stabilizing at its final position (4 and *c*). This behaviour resembles the sedimentation of a particle in a stagnant fluid at medium Reynolds numbers (Feng *et al.* 1994), and is further evidence of the strong wall effect at large slip velocities. It has been reported that stronger oscillatory behaviour (even undamped) occurs at large density differences (Denson *et al.* 1966; Brenner 1966).

The reversal predicted by our simulation, i.e. the equilibrium position of particles with large lead velocities moves back toward the centreline, has not been corroborated experimentally. The lack of experimental support may be related to the fact that this situation involves particle motion superposed onto fluid motion, and cannot be observed unless the test section is extremely long.

It should be pointed out that although the scenario of particle migration in shear flow fields is more or less clear now, we are unable to take quantitative account of the effects of all the parameters in terms of, say, a few dimensionless groups. In this sense, direct comparisons between numerical, experimental and analytical results will require further work.

4. Conclusions

Based on the results and discussions presented in this paper, the following conclusions can be drawn for the parameter ranges covered in this study:

1. For the lateral migration of a neutrally buoyant circular particle in a planar Couette shear flow, the centreline of the channel is a stable equilibrium position.

2. The motion of a non-neutrally buoyant particle in a Couette flow depends on the magnitude of the buoyancy force. When the density difference is small, the equilibrium position is near the stationary wall if the particle leads the local fluid, and near the moving wall if the particle lags. When the density difference is large enough, the equilibrium position shifts toward the centreline, irrespective of whether the particle is lighter or heavier than the fluid.

3. The Segré–Silberberg effect for a neutrally buoyant particle in a planar Poiseuille flow is simulated. The equilibrium position is closer to the wall for higher flow speed.

4. The motion of a non-neutrally buoyant particle in a Poiseuille flow depends on the magnitude of the buoyancy force. When the density difference is small, the equilibrium position is either near the wall or near the centreline, depending on whether the particle leads or lags the local fluid. When the density difference is large enough, the equilibrium position shifts toward the centreline, irrespective of whether the particle is lighter or heavier than the fluid.

5. Three mechanisms are identified as responsible for the lateral migration in a Couette flow: wall repulsion due to lubrication, inertial lift related to shear slip and a lift due to particle rotation. For a Poiseuille flow, an additional mechanism is a lift force due to the curvature of the undisturbed velocity profile. All the cases of lateral migration listed above can be explained in terms of these mechanisms.

6. These lateral forces are shown to be related to the flow field around the particle. Stagnation pressure on the surface of the particle is particularly important in determining the direction of migration.

7. The conclusions of perturbation theories agree qualitatively with our simulations for the motion of neutrally buoyant particles in Couette and Poiseuille flows. For non-neutrally buoyant particles, the reversal observed in our simulation is different from the predictions of the perturbation theory of Vasseur & Cox (1976).

8. Comparison with experimental data is qualitatively satisfactory in all cases except the reversal behaviour, which has not been experimentally observed. The comparison also reveals some misunderstanding and mis-interpretation in the literature.

This work was supported by the NSF, Fluid, Particulate and Hydraulic Systems; by the US Army, Mathematics and AHPCRC; by the DOE, Department of Basic Energy Sciences and the Minnesota Supercomputer Institute. H.H.H. acknowledges the partial support from the NSF through Laboratory for Research on the Structure of Matter at the University of Pennsylvania and from the Research Foundation of the University of Pennsylvania. The authors wish to thank Messrs. Todd Hesla, Adam Huang and Yijian Huang for helpful discussions.

REFERENCES

Aoki, H, Kurosaki, Y. & Anzai, H. 1979 Study on the tubular pinch effect in a pipe flow. I. Lateral migration of a single particle in laminar Poiseuille flow. *Bull. JSME* **22**, 206.

Brenner, H. 1966 Hydrodynamic resistance of particles at small Reynolds numbers. *Adv. Chem. Engng* **6**, 287.

Bretherton, F. P. 1962*a* Slow viscous motion round a cylinder in a simple shear. *J. Fluid Mech.* **12**, 591.

Bretherton, F. P. 1962*b* The motion of rigid particles in a shear flow at low Reynolds number. *J. Fluid Mech.* **14**, 284.

Cox, R. G. 1965 The steady motion of a particle of arbitrary shape at small Reynolds numbers. *J. Fluid Mech.* **23**, 625.

Cox, R. G. & Brenner, H. 1968 The lateral migration of solid particles in Poiseuille flow. Part 1. Theory. *Chem. Engng Sci.* **23**, 147.

Cox, R. G. & Hsu, S. K. 1977 The lateral migration of solid particles in a laminar flow near a plane. *Intl. J. Multiphase Flow* **3**, 201.

Cox, R. G. & Mason, S. G. 1971 Suspended particles in fluid flow through tubes. *Ann. Rev. Fluid Mech.* **3**, 291.

Cox, R. G., Zia, I. Y. & Mason, S. G. 1968 Particle motions in sheared suspensions. XXV. Streamlines around cylinders and spheres. *J. Colloid Interface Sci.* **27**, 7.

Denson, C. D., Christiansen, E. B. & Salt, D. L. 1966 Particle migration in shear fields. *AIChE J.* **12**, 589.

Feng, J., Hu, H. H. & Joseph, D. D. 1994 Direct simulation of initial value problems for the motion of solid bodies in a Newtonian fluid. Part 1. Sedimentation. *J. Fluid Mech.* **261**, 95.

Feuillebois, F. 1989 Some theoretical results for the motion of solid spherical particles in a viscous fluid. In *Multiphase Science and Technology* (ed. G. F. Hewitt *et al.*), vol. 4, p. 583. Hemisphere.

Goldsmith, H. L. & Mason, S. G. 1966 The microrheology of dispersions. In *Rheology, Theory and Applications* (ed. F. R. Eirich), vol. 4, p. 85. Academic.

HALOW, J. S. & WILLS, G. B. 1970*a* Radial migration of spherical particles in Couette systems. *AIChE J.* **16**, 281.

HALOW, J. S. & WILLS, G. B. 1970*b* Experimental observations of sphere migration in Couette systems. *Indust. Engng Chem. Fundam.* **9**, 603.

HAPPEL, J. & BRENNER, H. 1965 *Low Reynolds Number Hydrodynamics.* Prentice-Hall.

HO, B. P. & LEAL, L. G. 1974 Inertial migration of rigid spheres in two-dimensional unidirectional flows. *J. Fluid Mech.* **65**, 365.

HU, H. H., CROCHET, M. J. & JOSEPH, D. D. 1992 Direct simulation of fluid particle motions. *Theor. Comput. Fluid Dyn.* **3**, 285.

HUANG, Y., FENG, J. & JOSEPH, D. D. 1994 The turning couples on an elliptic particle settling in a vertical channel. *J. Fluid Mech.* **271**, 1.

JEFFERY, R. C. & PEARSON, J. R. A. 1965 Particle motion in laminar vertical tube flow. *J. Fluid Mech.* **22**, 721.

KARNIS, A., GOLDSMITH, H. L. & MASON, S. G. 1966 The flow of suspensions through tubes. Part 5: Inertial effects. *Can. J. Chem. Engng.* **44**, 181.

LEAL, L. G. 1980 Particle motion in a viscous fluid. *Ann. Rev. Fluid Mech.* **12**, 435.

LIU, Y.J., NELSON, J., FENG, J. & JOSEPH, D. D. 1993 Anomalous rolling of spheres down an inclined plane. *J. Non-Newtonian Fluid Mech.* **50**, 305.

MCLAUGHLIN, J. B. 1991 Integral migration of a small sphere in linear shear flow. *J. Fluid Mech.* **224**, 261.

MCLAUGHLIN, J. B. 1993 The lift on a small sphere in wall-bounded linear shear flows. *J. Fluid Mech.* **246**, 249.

OLIVER, D. R. 1962 Influence of particle rotation on radial migration in the Poiseuille flow of suspensions. *Nature* **194**, 1269.

REPETTI, R. V. & LEONARD, E. F. 1964 Segré–Silberberg annulus formation: a possible explanation. *Nature* **203**, 1346.

REPETTI, R. V. & LEONARD, E. F. 1966 Physical basis for the axial accumulation of red blood cells. *Chem. Engng Prog. Symp. Ser.* **62**, 80.

RUBINOW, S. I. & KELLER, J. B. 1961 The transverse force on a spinning sphere moving in a viscous fluid. *J. Fluid Mech.* **11**, 447.

SAFFMAN, P. G. 1965 The lift on a small sphere in a slow shear flow. *J. Fluid Mech.* **22**, 385.

SCHONBERG, J. A. & HINCH, E. J. 1989 Inertial migration of a sphere in Poiseuille flow. *J. Fluid Mech.* **203**, 517.

SEGRÉ, G. & SILBERBERG, A. 1961 Radial Poiseuille flow of suspensions. *Nature* **189**, 209.

SEGRÉ, G. & SILBERBERG, A. 1962 Behaviour of macroscopic rigid spheres in Poiseuille flow. Part 1. *J. Fluid Mech.* **14**, 115.

TACHIBANA, M. 1973 On the behavior of a sphere in the laminar tube flows. *Rheol. Acta* **12**, 58.

UNVERDI, S. O. & TRYGGVASON, G. 1992 A front-tracking method for viscous, incompressible, multi-fluid flows. *J. Comput. Phys.* **100**, 25.

VASSEUR, P. & COX, R. G. 1976 The lateral migration of a spherical particle in two-dimensional shear flows. *J. Fluid Mech.* **78**, 385.

VASSEUR, P. & COX, R. G. 1977 The lateral migration of spherical particles sedimenting in a stagnant bounded fluid. *J. Fluid Mech.* **80**, 561.